

# Optimal quadratic binding for relational reasoning in vector symbolic neural architectures

Naoki Hiratani<sup>1\*</sup>, Haim Sompolinsky<sup>1,2</sup>

<sup>1</sup>Center for Brain Science, Harvard University, Cambridge MA 02138, USA

<sup>2</sup>Edmond and Lily Safra Center for Brain Sciences, Hebrew University, Jerusalem 91904, Israel

## Abstract

Binding operation is fundamental to many cognitive processes, such as cognitive map formation, relational reasoning, and language comprehension. In these processes, two different modalities, such as location and objects, events and their contextual cues, and words and their roles, need to be bound together, but little is known about the underlying neural mechanisms. Previous works introduced a binding model based on quadratic functions of bound pairs, followed by vector summation of multiple pairs. Based on this framework, we address following questions: Which classes of quadratic matrices are optimal for decoding relational structures? And what is the resultant accuracy? We introduce a new class of binding matrices based on a matrix representation of octonion algebra, an eight-dimensional extension of complex numbers. We show that these matrices enable a more accurate unbinding than previously known methods when a small number of pairs are present. Moreover, numerical optimization of a binding operator converges to this octonion binding. We also show that when there are a large number of bound pairs, however, a random quadratic binding performs as well as the octonion and previously-proposed binding methods. This study thus provides new insight into potential neural mechanisms of binding operations in the brain.

## 1 Introduction

In many cognitive tasks, the brain has to construct a compositional representation by binding various properties of things like objects, events, or words. However, little is known about how the brain solves this binding problem (Feldman, 2013). For example, the scene depicted in Figure 1A is decomposed into a set of object-location pairs as

$$[\text{scene}] = \{(\text{pink-cube}, \text{left}), (\text{green-pyramid}, \text{middle}), (\text{red-cylinder}, \text{right})\}. \quad (1)$$

This compositional representation of the object-location pairs is crucial for scene understanding. For instance, by having this representation in your working memory, you can answer questions like “what is the left-most object?” (answer: pink-cube), “what is the position of the red-cylinder?” (answer: right) from your memory. However, it remains elusive how the brain binds neural representations of objects and locations and creates a compositional representation. Similarly, in the context of natural language processing, a sentence is interpreted as a set of word-position pairs:

$$[\text{“Man bites dog”}] = \{(\text{“man”}, 1), (\text{“bites”}, 2), (\text{“dog”}, 3)\}. \quad (2)$$

Here, the syntactic position information paired with the words differentiate the sentence “man bites dog” from “dog bites man”, implying that the binding of words and their syntactic positions is essential for language processing. Similar compositional representations are also suggested to be essential for relational inference, object-based navigation, and episodic memory formation (Eliasmith et al., 2012; Whittington et al., 2020). Moreover, the binding problem is also an important topic in machine learning literature (Greff et al., 2020), particularly in knowledge graph construction (Socher et al., 2013; Nickel et al., 2016), and relational reasoning (Johnson et al., 2017; Santoro et al., 2017).

---

\*n.hiratani@gmail.com

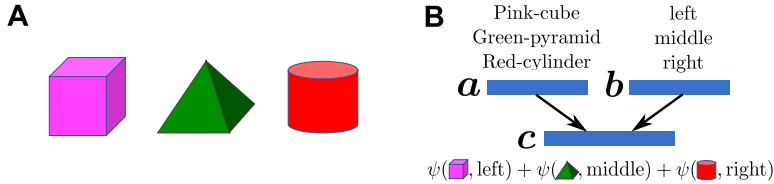


Figure 1: Schematics of the binding problem. **A**) A scene with three objects: pink-cube (left), green-pyramid (middle), and red-cylinder (right). **B**) Representation of the scene in VSA (vector symbolic architecture). Vector representation of objects ( $\mathbf{a}$ ) and their positions ( $\mathbf{b}$ ) are combined into a compositional representation of the entire scene ( $\mathbf{c}$ ).

Mathematically speaking, this is a problem of vector representation construction. Let us consider a vector representation of a set of pairs  $S = \{(\mathbf{a}_\mu, \mathbf{b}_\mu)\}_{\mu=1}^L$ , where  $L$  is the number of the pairs, and  $\mathbf{a}$  and  $\mathbf{b}$  are  $N$ -dimensional vectors. For instance, in the case of the scene recognition depicted in Figure 1A,  $\mathbf{a}_1$  is a vector representation of “pink-cube”, while  $\mathbf{b}_1$  is a representation of the position “left”, and so on (Fig. 1B). In the brain, the number of neurons recruited for a representation of an object or its position is expectedly large, whereas previous human studies indicate that the number of pairs,  $L$ , the brain can hold in the short-term memory is less than ten (Miller, 1956; Cowan, 2001). Therefore, we will mainly focus on the parameter regime where  $1 \lesssim L \ll N$  is satisfied.

Previous works proposed the vector symbolic architecture (VSA) as a biological-plausible solution for the binding problem (Smolensky, 1990; Plate, 1995; Gayler, 2004; Kanerva, 2009). In particular, VSA is capable of instantaneous construction of compositional structures essential for linguistic processing (Gayler, 2004). In the VSA framework, a vector representation of a set  $S = \{(\mathbf{a}_\mu, \mathbf{b}_\mu)\}_{\mu=1}^L$  is constructed by:

$$\begin{aligned} \mathbf{c}_\mu &= \psi(\mathbf{a}_\mu, \mathbf{b}_\mu) & : \text{binding} \\ \mathbf{c} &= \sum_{i=1}^L \mathbf{c}_\mu & : \text{bundling} \end{aligned} \quad (3)$$

where  $\mathbf{c}$  is a  $N_c$ -dimensional vector, and  $\psi$  is a non-linear mapping  $\psi : \mathbb{R}^N \times \mathbb{R}^N \rightarrow \mathbb{R}^{N_c}$ . This means that we first create a representation of a pair  $(\mathbf{a}_\mu, \mathbf{b}_\mu)$  by a non-linear mapping  $\psi(\mathbf{a}_\mu, \mathbf{b}_\mu)$ , then generate a representation of the set  $S$  by summing up the representation of the pairs (Fig. 1B). By constructing a representation of a set by taking the sum over pairs, the length of vector  $\mathbf{c}$  stays constant regardless of the cardinality of the set  $L$ . This is a desirable property when we consider population coding by a fixed number of neurons. However, it also causes interference between different pairs, as we will see.

In this paper, we study how we should choose the binding operator  $\psi$ . The answer depends on the objective, but it is often desirable for  $\mathbf{c}$  to maximize the unbinding performance. In other words, we should be able to retrieve  $\mathbf{a}_\mu$  from  $\mathbf{c}$  using  $\mathbf{b}_\mu$  as a query, and vice versa. In our example (Fig. 1A), representation of the scene,  $\mathbf{c}$ , should enable us to answer a question like “what is the left-most object?” (answer: pink-cube) or “what is the position of the red-cylinder?” (answer: right).

Previous works introduced two binding mechanisms for VSA architecture, the holographic reduced representation (HRR) (Plate, 1995) and the tensor product representation (Smolensky, 1990), among others (Kanerva et al., 1997; Gallant and Okaywe, 2013; Gosmann and Eliasmith, 2019; Frady et al., 2020). HRR is noisy, but the size of composition  $\mathbf{c}$  is the same with its elements  $\mathbf{a}, \mathbf{b}$  (i.e.,  $N_c = N$ ). On the other hand, the tensor product representation is more accurate, but it requires  $N_c = N^2$  neurons for representing a composition (see Appendix C.1 and C.2 for the details of the two binding methods). Though their properties have been studied previously (Plate, 1997; Schlegel et al., 2020; Steinberg and Sompolinsky, 2022), it remains elusive if HRR and the tensor product representation are the optimal binding under  $N_c = N$  and  $N_c = N^2$  respectively. Moreover, little is known on how we should construct a binding operator under various composition sizes  $N_c$  and how the minimum achievable error scales with the number of bound pairs  $L$ . Below, we address these questions under a quadratic parameterization of the binding operators. We found that at  $L \sim O(1)$ , there is a novel binding algorithm based on a matrix representation of the octonion algebra that significantly outperforms HRR and its extension. We also show that when  $L \gg 1$  and  $N_c \ll N^2$ , there is no quadratic binding method that significantly outperforms a random binding method.

## 2 Quadratic binding

Below, we introduce a specific class of binding operators that has a quadratic form. More specifically, using an  $N \times N \times N_c$  tensor  $P$ , we define the  $k$ -th element of a representation of set  $S = \{(\mathbf{a}_\mu, \mathbf{b}_\mu)\}_{\mu=1}^L$  as

$$c_k = \sum_{\mu=1}^L \sum_{i=1}^N \sum_{j=1}^N P_{ijk} a_i^\mu b_j^\mu, \quad (4)$$

for  $k = 1, \dots, N_c$ , where  $a_i^\mu$  is the  $i$ -th element of vector  $\mathbf{a}_\mu$ . There are several motivations for why we consider this quadratic parameterization. First, assuming that the norm of the vectors is constant ( $\|\mathbf{a}\|^2 = \|\mathbf{b}\|^2 = N$ ), many previously proposed binding operators, such as HRR and the tensor product representation are written as examples of quadratic binding. For instance, if we set  $P_{ijk} = \delta_{[i+j]_N, k}$  with  $[i+j]_N \equiv i+j \pmod{N}$ , we recover HRR,  $c_k = \sum_{\mu} \sum_i a_i^\mu b_{[k-i]_N}^\mu$  (see Appendix C.1). Moreover, when  $\mathbf{a}$  and  $\mathbf{b}$  are random Gaussian variables, the quadratic parameterization should be enough to capture the statistical relationship between  $\mathbf{a}$  and  $\mathbf{b}$ . Thirdly, this formulation is simple enough to be biologically plausible, though the biological substrates for the multiplication are not yet fully understood.

From this vector representation  $\mathbf{c}$ , we consider unbinding of a vector using its bound pair as a query. For example, to answer the question ‘‘what is the left-most object?’’ from a vector representation of the scene depicted in Fig. 1A, we need to unbind ‘‘pink-cube’’ from representation  $\mathbf{c}$  by using the position ‘‘left’’ as a query. Here, we also restrict this unbinding operation onto a quadratic form. Unbinding of  $\mathbf{a}_1$  with a query  $\mathbf{b}_1$  is defined by

$$\hat{\mathbf{a}}_i^1 = \sum_{j=1}^N \sum_{k=1}^{N_c} Q_{ijk} b_j^1 c_k, \quad (5)$$

where  $Q$  is an  $N \times N \times N_c$  tensor. Similarly, using an  $N \times N \times N_c$  tensor  $R$ , unbinding of  $\mathbf{b}_1$  with  $\mathbf{a}_1$  is defined by

$$\hat{\mathbf{b}}_j^1 = \sum_{i=1}^N \sum_{k=1}^{N_c} R_{ijk} a_i^1 c_k. \quad (6)$$

Our objective is to find a set of tensors  $P, Q, R$  that achieves the best unbinding performance. Using the mean-squared error as the loss, we define the unbinding error of  $\mathbf{a}_1$  and  $\mathbf{b}_1$  as

$$\ell_a(P, Q) \equiv \frac{1}{N} \left\langle \|\mathbf{a}_1 - \hat{\mathbf{a}}_1\|^2 \right\rangle_{p(S)}, \quad (7)$$

and

$$\ell_b(P, R) \equiv \frac{1}{N} \left\langle \|\mathbf{b}_1 - \hat{\mathbf{b}}_1\|^2 \right\rangle_{p(S)}. \quad (8)$$

Below, we consider the case when  $\mathbf{a}$  and  $\mathbf{b}$  are sampled from an i.i.d Gaussian distribution  $N(0, I_N)$ . This assumption is introduced partially for analytical tractability, but we would also expect the input vectors  $\mathbf{a}$  and  $\mathbf{b}$  to be whitened in the preprocessing.

Inserting Eq. 4 and Eq. 5 into the loss  $\ell_a$  (Eq. 7), we get

$$\ell_a = \frac{1}{N} \left\langle \sum_{i=1}^N \left( a_i^1 - \sum_{\mu=1}^L \sum_{j=1}^N \sum_{l=1}^N \sum_{m=1}^N \left[ \sum_{k=1}^{N_c} Q_{ijk} P_{lmk} \right] b_j^1 b_m^\mu a_i^\mu \right)^2 \right\rangle_{p(\mathbf{a}, \mathbf{b})}. \quad (9)$$

Because the error depends only on the tensor product of  $P$  and  $Q$  over index  $k$ , there is an invariance in the choice of  $P$  and  $Q$ . If we define  $\tilde{Q}_{ijk} = \sum_n Q_{ijn} A_{nk}$  and  $\tilde{P}_{lmk} = \sum_n P_{lmn} [A^{-1}]_{kn}$  with an  $N_c \times N_c$  invertible matrix  $A$ , we get  $\sum_k Q_{ijk} P_{lmk} = \sum_k \tilde{Q}_{ijk} \tilde{P}_{lmk}$ , indicating that the choice of the optimal  $P$  and  $Q$  is not unique. Taking the expectation over  $\mathbf{a}$  and  $\mathbf{b}$ , the equation above is rewritten as (see Appendix A.1)

$$\ell_a = 1 - \frac{2}{N} \sum_i \text{tr} [P_i Q_i^T] + \frac{1}{N} \sum_i \sum_l \left( (\text{tr} [P_l Q_i^T])^2 + \text{tr} [P_l Q_i^T (L \cdot Q_i P_l^T + P_l Q_i^T)] \right), \quad (10)$$

where all summations run from 1 to  $N$ , and  $P_i$  and  $Q_i$  are  $N \times N$  matrices corresponding to the  $i$ -th component of tensors  $P$  and  $Q$ , respectively:

$$[P_i]_{jk} = P_{ijk}, \quad [Q_i]_{jk} = Q_{ijk}. \quad (11)$$

Similarly, by taking the expectation over  $\mathbf{a}$  and  $\mathbf{b}$ , the decoding loss of  $\mathbf{b}$  is given as

$$\ell_b = 1 - \frac{2}{N} \sum_i \text{tr} [P_i R_i^T] + \frac{1}{N} \sum_i \sum_l (\text{tr} [P_i R_i^T R_l P_l^T] + \text{tr} [P_l R_l^T (L \cdot R_i P_l^T + R_l P_i^T)]), \quad (12)$$

where  $[R_i]_{jk} = R_{ijk}$ .

### 3 The binding solutions under $L = 1$

How should we choose binding operator  $P$  and unbinding operators  $Q, R$  to minimize the loss  $\ell_a$  and  $\ell_b$ ? Let us start from a simple scenario where only one pair is bound (i.e.,  $L = 1$ ), and the size of the composition  $\mathbf{c}$  is the same with its elements  $\mathbf{a}$  and  $\mathbf{b}$  (i.e.,  $N_c = N$ ). In this scenario, there is actually a trivial non-quadratic lossless algorithm in which binding and unbinding are performed by  $\mathbf{c} = \mathbf{a} + \mathbf{b}$  and  $\hat{\mathbf{a}} = \mathbf{c} - \mathbf{b}$ , which we call the sum binding. However, this strategy scales badly to  $L > 1$  as we will see later. Below, we first investigate the solution numerically using a fixed-point algorithm, then subsequently, study a sufficient condition for a local minimum of  $\ell_a$  and  $\ell_b$  analytically.

#### 3.1 Numerical optimization of the binding tensor

To investigate the solution space of the quadratic binding operators, we first optimize the binding operators  $P, Q, R$  numerically for both  $\ell_a$  and  $\ell_b$  using a fixed-point algorithm. Taking the gradient of  $\ell_a$  with respect to  $P_l$  and rewriting this equation in a tensor form, the fixed-point condition is given as (see Appendix A.2 for the details)

$$\frac{\partial \ell_a}{\partial P_l} = 0 \Leftrightarrow Q_{ljk} = \sum_{m,n} \Gamma_{[jN+k],[mN+n]}^q P_{lmn}, \quad (13)$$

for  $j, k = 1, \dots, N$ , where  $\Gamma^q$  is a  $N^2 \times N^2$  matrix defined as

$$\Gamma_{[jN+k],[mN+n]}^q \equiv \sum_i \left( \delta_{jm} \sum_{\beta} Q_{i\beta k} Q_{i\beta n} + Q_{ijk} Q_{imn} + Q_{ijn} Q_{imk} \right). \quad (14)$$

Therefore, for a given unbinding tensor  $Q$ , the binding tensor  $P$  satisfying  $\frac{\partial \ell_a}{\partial P_l} = 0$  is given as

$$\text{Vec} [P_l] = (\Gamma^q)^{-1} \text{Vec} [Q_l], \quad (15)$$

where  $\text{Vec} [P_l]$  and  $\text{Vec} [Q_l]$  are the vector representation of  $N \times N$  matrices  $P_l$  and  $Q_l$ , respectively. From a similar calculation, for a given binding tensor  $P$ , the fixed point of  $\ell_a$  with respect to  $Q$  is given as

$$\text{Vec} [Q_l] = (\Gamma^{pa})^{-1} \text{Vec} [P_l], \quad (16)$$

where  $\Gamma^{pa}$  is an  $N^2 \times N^2$  matrix that only depends on  $P$ . Moreover, we can update  $P$  and  $R$  with respect to  $\ell_b$  by

$$\text{Vec} [\check{P}_m] = (\Gamma^r)^{-1} \text{Vec} [\check{R}_m], \quad \text{Vec} [\check{R}_j] = (\Gamma^{pb})^{-1} \text{Vec} [\check{P}_j] \quad (17)$$

respectively, where  $\check{R}_m$  and  $\check{P}_m$  are defined as  $[\check{R}_m]_{l,k} = R_{lmk}$  and  $[\check{P}_m]_{l,k} = P_{lmk}$ , and  $\Gamma^r$  and  $\Gamma^{pb}$  are  $N^2 \times N^2$  matrices (defined at Eqs. 62 and 65 in Appendix A.2). Therefore, we can perform an iterative optimization of tensors  $P, Q, R$  with respect to both  $\ell_a$  and  $\ell_b$  by the fixed-point algorithm described in Algorithm 1.

Figures 2A and B describe the learning curves of this algorithm from ten random initializations. Both decoding errors  $\ell_a$  and  $\ell_b$  first plateau around  $\ell_a \approx 0.35$ , then converge to  $1/5$ , robustly. To evaluate the performance of this

---

**Algorithm 1** A fixed-point algorithm of  $P, Q, R$  optimization
 

---

```

randomly initialize  $P, Q, R$ 
for t in 1...T:
     $\text{Vec}[Q_i] = (\Gamma^{pa})^{-1} \text{Vec}[P_i]$  for  $i = 1, \dots, N$ 
     $\text{Vec}[P_i] = (\Gamma^q)^{-1} \text{Vec}[Q_i]$  for  $i = 1, \dots, N$ 
     $\text{Vec}[\tilde{R}_j] = (\Gamma^{pb})^{-1} \text{Vec}[\tilde{P}_j]$  for  $j = 1, \dots, N$ 
     $\text{Vec}[\tilde{P}_j] = (\Gamma^r)^{-1} \text{Vec}[\tilde{R}_j]$  for  $j = 1, \dots, N$ 
  
```

---

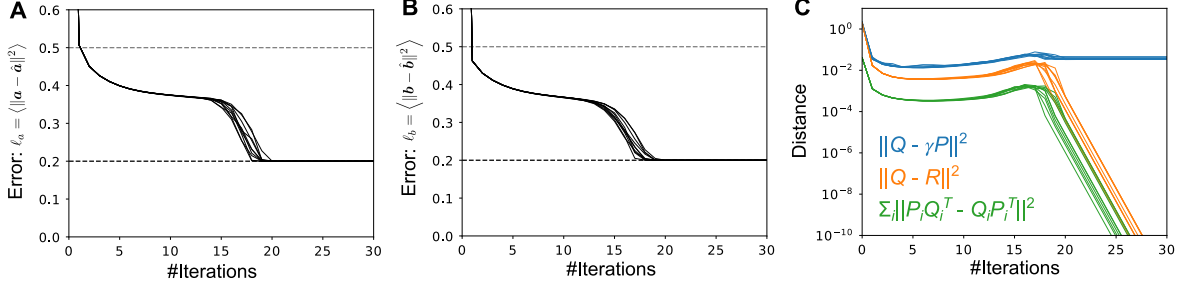


Figure 2: Iterative optimization of binding operators  $P, Q, R$  under  $N = 48$  and  $L = 1$ . **A)** Learning dynamics of the fixed-point algorithm from random initializations. Here, we evaluated the loss  $\ell_a$  directly from Eq. 10. Each line represents a learning curve of the decoding error  $\ell_a$  from a random initialization. The black dashed line represents the error after convergence, and gray dashed line is the error under HRR. **B)** The same as **A**, but the y-axis is  $\ell_b$ , not  $\ell_a$ . **C)** Change in distance measures during learning. We defined the distances using the Frobenius norm as  $\|Q - \gamma P\|^2 \equiv \sum_{i,j,k} (Q_{ijk} - \gamma P_{ijk})^2$  where  $\gamma = \frac{\max Q}{\max P}$ ,  $\|Q - R\|^2 \equiv \sum_{i,j,k} (Q_{ijk} - R_{ijk})^2$ , and  $\sum_i \|P_i Q_i^T - Q_i P_i^T\|^2 \equiv \sum_{ijk} \left( [P_i Q_i^T]_{jk} - [Q_i P_i^T]_{kj} \right)^2$ .

---

optimized binding operator, we compare it with HRR (Plate, 1995), a binding method using the circular convolution (see Appendix C.1). Under HRR, the binding and the unbinding operators are given as,

$$P_{ijk} = Q_{ijk} = R_{ijk} = \frac{1}{\sqrt{2(N+1)}} \delta_{[i+j]_N, k}, \quad (18)$$

where  $[x]_N \equiv x \pmod{N}$ , and the decoding error is  $\ell_a = \ell_b = 1/2$  under a large  $N$  (gray dashed lines in Figs. 2A and B). This means that the numerically optimized binding operator achieves a better decoding performance than HRR under  $L = 1$ .

To see if the numerically optimized binding operators  $P, Q, R$  have some specific structures, we next investigate the values of  $P, Q, R$  after learning. Firstly, upon optimization,  $Q$  and  $R$  converge to the same values (i.e.,  $Q = R$ ; orange lines in Fig. 2C), but  $P \neq Q, R$  even under a rescaling (blue lines; here we plotted a normalized distance  $\sum_{ijk} (Q_{ijk} - \gamma P_{ijk})^2$  with  $\gamma = \frac{\max Q}{\max P}$ ). Moreover, the matrix products  $P_1 Q_1^T, \dots, P_N Q_N^T$  converge to symmetry matrices after the optimization (green lines).

Elements of matrix  $P_i$  look random even after an optimization (Fig. 3A; here we plotted  $P_1, \dots, P_5$  out of  $N = 48$  matrices  $P_1, \dots, P_{48}$ ) potentially due to an invariance in the solution space, and the same is true for the elements of  $Q_i$  (Fig. 3B). To untangle the invariance and extract the hidden structure in  $P, Q, R$ , we process the tensors in the following way:

1. Because  $P_1 Q_1^T$  converges to a symmetric matrix, we can decompose it as  $P_1 Q_1^T = U_1 \Sigma_1 U_1^T$  where  $U_1$  is an  $N \times N$  orthogonal matrix, and  $\Sigma_1$  is an  $N \times N$  diagonal matrix.
2. We introduce an  $N \times N$  matrix  $A_1$  by  $A_1 \equiv P_1^{-1} U_1 \Sigma_1^{1/2}$ .

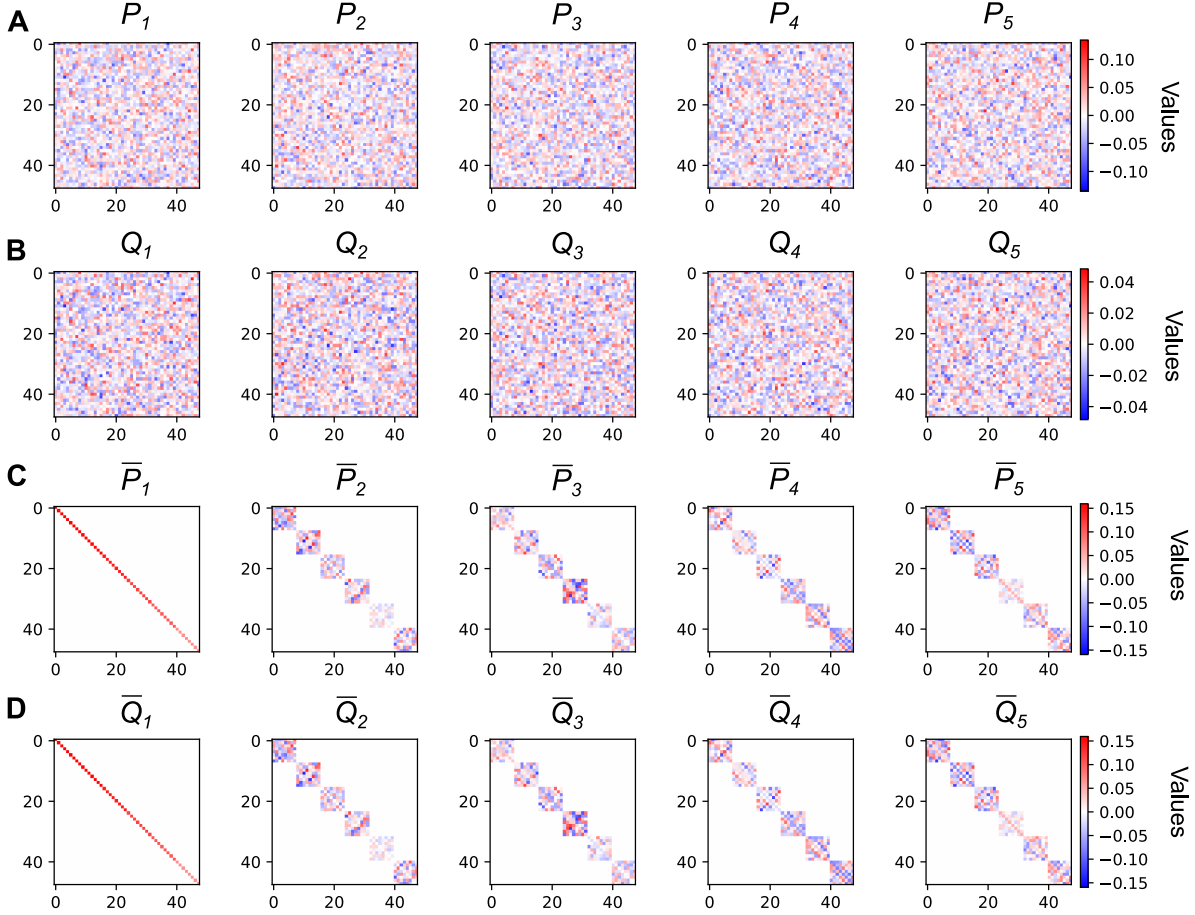


Figure 3: Binding matrices obtained after the convergence from one random initialization ( $N = 48$ ,  $L = 1$ ). **A)**  $P_1, \dots, P_5$  (of  $P_1, \dots, P_{48}$ ) after 100 iterations of the numerical optimization. **B)**  $Q_1, \dots, Q_5$  after the numerical optimization. **C, D)** The same as the binding matrices depicted in panels **A** and **B** respectively, but transformed into a space where  $\bar{P}_1$  is diagonal.

3. We transform the binding matrices  $P_i$  by  $\bar{P}_i = U_1^T P_i A_1$  for  $i = 1, \dots, N$ .

This transformation cancels out the invariance in the choice of  $P$  and  $Q$ , and maps  $P_i$  onto the space where  $\bar{P}_1$  is a diagonal matrix ( $\bar{P}_1 = \Sigma_1^{1/2}$ ). After this preprocessing, we found an  $8 \times 8$  block structure in all  $\bar{P}_i$  (Fig. 3C; we plotted  $\bar{P}_1, \dots, \bar{P}_5$  out of  $\bar{P}_1, \dots, \bar{P}_{48}$  as before). Note that, there is no constraint that enforces the  $8 \times 8$  structure in the learning algorithm nor the data processing, except that  $N = 48$  is a multiple of eight. Similarly, by preprocessing  $Q_i$  by  $\bar{Q}_i = U_1^T Q_i B_1$  with  $B_1 = Q_1^{-1} U_1 \Sigma_1^{1/2}$ , we recover the  $8 \times 8$  block structure (Fig. 3D). Moreover,  $\bar{P}_i = \bar{Q}_i$  is satisfied for all  $i = 1, \dots, N$  (compare Figs. 3C and 3D). Notably,  $\bar{P}_i \bar{Q}_i^T$  is rewritten as

$$\bar{P}_i \bar{Q}_i^T = U_1^T P_i P_1^{-1} U_1 \Sigma_1 U_1^T (Q_1^T)^{-1} Q_i U_1^T = U_1^T P_i Q_i^T U_1. \quad (19)$$

Therefore, under the transformation  $\{P_i, Q_i\} \rightarrow \{\bar{P}_i, \bar{Q}_i\}$ , the loss  $\ell_a$  (Eq. 10) is preserved. This means that, up to a linear transformation with an orthogonal matrix, these numerically optimized operators are symmetric ( $Q = R$  and  $\bar{P} = \bar{Q}$ ) and have a hidden  $8 \times 8$  block structure. In the rest of the section, we discuss why we see the  $8 \times 8$  structure in the optimized binding operators from an algebraic perspective.

### 3.2 Composition algebra-based solution for the quadratic binding problem

Our numerical optimization indicates that there is a non-trivial binding method with a  $8 \times 8$  block diagonal structure that outperforms a previously proposed method. To understand the origin of the  $8 \times 8$  block structure, we next analytically study a sufficient condition for a local minimum of both  $\ell_a$  and  $\ell_b$ . Below, we introduce  $P = Q = R$  constraint for the binding and unbinding tensors. This is motivated by the symmetric structure we saw in the numerical optimization (Figs. 2C and 3CD). Note that, two popular binding methods, HRR and the tensor product representation, also satisfy this  $P = Q = R$  constraint (see Appendix C). Taking the gradient of  $\ell_a$  under the symmetric constraint  $P = Q$ , the fixed-point condition is given as

$$P_i = \sum_{l=1}^N (\text{tr} [P_l P_i^T] I_N + P_l P_i^T + P_i P_l^T) P_l \quad (20)$$

for  $i = 1, \dots, N$ , where  $I_N$  is the size  $N$  identity matrix. Similarly, introducing  $P = R$  constraint, the fixed-point condition for  $\ell_b$  is written as

$$P_i = \sum_{l=1}^N (P_i P_l^T P_l + P_l P_i^T P_l + P_l P_l^T P_i). \quad (21)$$

What kind of  $P = \{P_1, P_2, \dots, P_N\}$  satisfies Eqs. 20 and 21? A sufficient condition for both Eqs. 20 and 21 is

$$P_l P_i^T + P_i P_l^T = 2\lambda \delta_{il} I_N, \quad (22)$$

for all  $i, l = 1, \dots, N$ , with the scaling factor  $\lambda = \frac{1}{N+2}$  (see Appendix B.1). This set of equations is known as the Hurwitz matrix equations. It has been proved that, there exists a family of  $N$  matrices of size  $N \times N$  that satisfies Eq. 22 only if  $N = 1, 2, 4, 8$ , and a solution is given by a real matrix representation of the composition algebra of dimension  $N$  (Shapiro, 2011). This means that, when binding two vectors  $\mathbf{a}, \mathbf{b}$  having the length  $N = 1, 2, 4, 8$ , you can locally minimize the decoding error by using a solution of the Hurwitz matrix equations as a binding operator  $P$ .

For instance, when  $N = 2$ , by setting

$$P_1 = \frac{1}{2} \begin{pmatrix} 1 & 0 \\ 0 & 1 \end{pmatrix}, P_2 = \frac{1}{2} \begin{pmatrix} 0 & 1 \\ -1 & 0 \end{pmatrix}, \quad (23)$$

Eq. 22 is satisfied. Then, from Eq. 4, binding of two (real) vectors  $\mathbf{a} = (a_1, a_2)$  and  $\mathbf{b} = (b_1, b_2)$  becomes

$$\mathbf{c} = \frac{1}{2} \begin{pmatrix} a_1 b_1 - a_2 b_2 \\ a_1 b_2 + a_2 b_1 \end{pmatrix}, \quad (24)$$

and unbinding of  $\mathbf{a}$  is given as  $\hat{\mathbf{a}} = \frac{b_1^2 + b_2^2}{4} (a_1, a_2)$ . Notably,  $P_1$  and  $P_2$  consist of a basis of a matrix representation of the complex numbers up to a scaling factor. Let us define a projection  $\phi : \mathbb{C} \rightarrow \mathbb{R}^2 \times \mathbb{R}^2$  by

$$\phi(x + iy) = 2(xP_1 + yP_2) = \begin{pmatrix} x & y \\ -y & x \end{pmatrix}. \quad (25)$$

Then, for two complex numbers  $a = a_1 + ia_2$  and  $b = b_1 + ib_2$ ,

$$\phi(a)\phi(b) = \begin{pmatrix} a_1 & a_2 \\ -a_2 & a_1 \end{pmatrix} \begin{pmatrix} b_1 & b_2 \\ -b_2 & b_1 \end{pmatrix} = \begin{pmatrix} a_1 b_1 - a_2 b_2 & a_1 b_2 + a_2 b_1 \\ -(a_1 b_2 + a_2 b_1) & a_1 b_1 - a_2 b_2 \end{pmatrix} = \phi(ab). \quad (26)$$

Thus, at  $N = 2$ , a matrix representation of the complex numbers provides a binding operator  $P = [P_1, P_2]$  that satisfies the fixed-point conditions (Eqs. 20 and 21). Similarly, at  $N = 4$ , we can construct a binding operator  $P = [P_1, P_2, P_3, P_4]$  using a matrix representation of the quaternions:

$$P_1 = \frac{1}{\sqrt{6}} \begin{pmatrix} 1 & 0 & 0 & 0 \\ 0 & 1 & 0 & 0 \\ 0 & 0 & 1 & 0 \\ 0 & 0 & 0 & 1 \end{pmatrix}, P_2 = \frac{1}{\sqrt{6}} \begin{pmatrix} 0 & 1 & 0 & 0 \\ -1 & 0 & 0 & 0 \\ 0 & 0 & 0 & 1 \\ 0 & 0 & -1 & 0 \end{pmatrix}, P_3 = \frac{1}{\sqrt{6}} \begin{pmatrix} 0 & 0 & 1 & 0 \\ 0 & 0 & 0 & -1 \\ -1 & 0 & 0 & 0 \\ 0 & 1 & 0 & 0 \end{pmatrix}, P_4 = \frac{1}{\sqrt{6}} \begin{pmatrix} 0 & 0 & 0 & 1 \\ 0 & 0 & 1 & 0 \\ 0 & -1 & 0 & 0 \\ -1 & 0 & 0 & 0 \end{pmatrix}. \quad (27)$$

Under this binding operator, the composition  $\mathbf{c}$  of the two vectors  $\mathbf{a}$  and  $\mathbf{b}$  is given as

$$\begin{aligned} c_1 &= \frac{1}{\sqrt{6}} (a_1 b_1 + a_2 b_2 + a_3 b_3 + a_4 b_4) \\ c_2 &= \frac{1}{\sqrt{6}} (a_1 b_2 - a_2 b_1 - a_3 b_4 + a_4 b_3) \\ c_3 &= \frac{1}{\sqrt{6}} (a_1 b_3 + a_2 b_4 - a_3 b_1 - a_4 b_2) \\ c_4 &= \frac{1}{\sqrt{6}} (a_1 b_4 - a_2 b_3 + a_3 b_2 - a_4 b_1) \end{aligned} \quad (28)$$

and using  $P$  as the unbinding tensor, from Eq. 5, we get

$$\hat{\mathbf{a}} = \frac{1}{6} (b_1^2 + b_2^2 + b_3^2 + b_4^2) \mathbf{a}. \quad (29)$$

Therefore, decoding of  $\mathbf{a}$  is faithful up to a constant scaling factor under this quaternion-based binding. Similarly, we can construct a binding operator based on a matrix representation of the octonions, an extension of the quaternions to  $N = 8$  dimensional space (see Appendix B.2). However, this is not true for  $N > 8$ , because Eq. 22 does not admit a solution.

### 3.3 Sparse $K$ -compositional bindings

Although solutions based on the composition algebra we discussed above are lossless, they cannot be directly extended to the case when  $N > 8$  because the Hurwitz matrix equations do not have a solution. Nevertheless, we can apply this binding in a block-wise manner. Let us define a family of matrices that satisfies the Hurwitz matrix equations (Eq. 22) as  $[A_1, A_2, \dots, A_K]$ , where  $K = 1, 2, 4$  or  $8$  and each  $A_k$  is a  $K \times K$  matrix. Suppose  $N = \dim(\mathbf{a})$  satisfies  $N = qK$  for a positive integer  $q$ . We define a sparse  $K$ -compositional binding by

$$P_i = \underbrace{O_K \oplus \dots \oplus O_K}_{\lfloor (i-1)/K \rfloor} \oplus A_{i \% K} \oplus O_K \oplus \dots \oplus O_K, \quad (30)$$

for  $i = 1, \dots, N$ , where  $O_K$  is the  $K \times K$  zero matrix,  $A \oplus B$  is the direct sum of matrices  $A$  and  $B$ ,  $\lfloor x \rfloor$  represents the largest integer smaller or equal to  $x$ , and  $x \% y$  is the remainder of  $x$  divided by  $y$  (for ease of notation, we define  $A_0 = A_K$ ). We denote this binding mechanism as the sparse  $K$ -compositional binding because it is a sparse implementation of the composition algebra of dimension  $K$ . For instance, if  $K = 2$  and  $q = 3$ , we get

$$P_1 = \begin{pmatrix} A_1 & O & O \\ O & O & O \\ O & O & O \end{pmatrix}, P_2 = \begin{pmatrix} A_2 & O & O \\ O & O & O \\ O & O & O \end{pmatrix}, P_3 = \begin{pmatrix} O & O & O \\ O & A_1 & O \\ O & O & O \end{pmatrix}, P_4 = \begin{pmatrix} O & O & O \\ O & A_2 & O \\ O & O & O \end{pmatrix}, \dots \quad (31)$$

When  $q = 1$ , they are matrix representations of the composition algebra we discussed in the previous section. Whereas under  $K = 1$ , we get a binding by the Hadamard product. Although  $P = [P_1, P_2, \dots, P_N]$  does not satisfy the Hurwitz matrix equations when  $q > 1$  ( $P_i P_i^T \neq \lambda I_N$ ), it satisfies the fixed-point condition, Eqs. 20 and 21 (see Appendix B.3). This means that a sparse  $K$ -compositional tensor  $P$  is a fixed-point solution of both  $\ell_a$  and  $\ell_b$ . The decoding error under this binding is given as

$$\ell_a = \ell_b = \frac{2}{K+2}. \quad (32)$$

This error is significantly smaller than that of HRR under  $K = 4$  and  $K = 8$  (Fig. 4A, purple and orange lines vs. blue line). In particular, under  $K = 8$ , we get  $\ell_a = \ell_b = 1/5$ , the same error we observed under a numerical optimization (compare Figs. 2A and B with Fig. 4A). It also explains why we found  $8 \times 8$  block structures (Figs. 3C and D). Among sparse  $K$ -compositional bindings,  $K = 8$  yields the smallest error because it is the largest matrix family that satisfies the Hurwitz matrix equations.

Using Cayley-Dickson construction (Baez, 2002), we can in principle construct sparse  $K$ -compositional binding tensors for  $K = 16$  (sedenions),  $32$  (trigintaduonions), and so on. However, it does not improve the unbinding performance (right side of Fig. 4B), because they do not satisfy the Hurwitz matrix equations. Thus, the binding



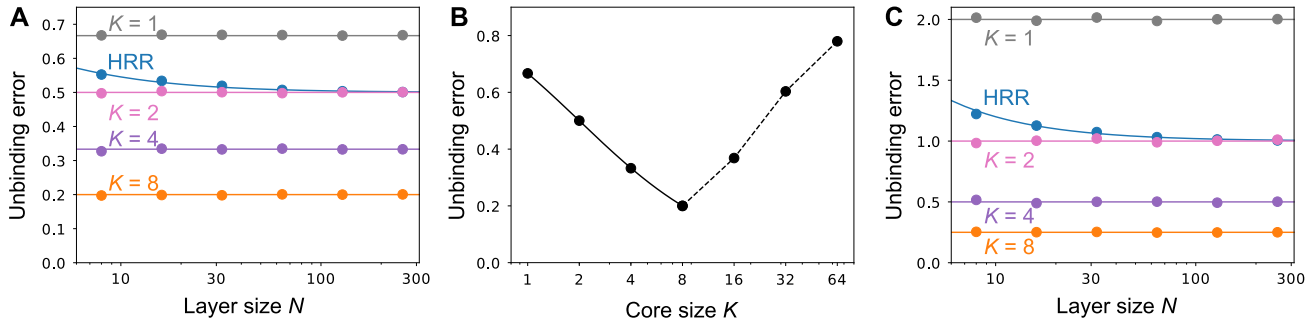


Figure 4: Performance of sparse  $K$ -compositional binding methods under  $L = 1$ . **A)** Decoding error  $\ell_a$  of sparse  $K$ -compositional binding methods with the core size  $K = 1, 2, 4, 8$  and the holographic reduced representation (HRR) under various layer sizes  $N$ . Points are simulations and lines are theory ( $\ell_a = 2/(K + 2)$  for  $K$ -compositional, and  $\ell_a = \frac{N+2}{2(N+1)}$  for HRR). **B)** Decoding error  $\ell_a$  of the sparse  $K$ -compositional binding methods with various core sizes  $K$  under  $N = 128$ . The solid line is  $\frac{2}{K+2}$ , while the dotted line is a linear interpolation. **C)** The same as **A**, except that the binding operators were normalized so that the amplitude of the signal is maintained in the unbinding. Points are simulations and lines are theory ( $\ell_a = 2/K$  for  $K$ -compositional, and  $\ell_a = 1 + \frac{2}{N}$  for HRR).

tensor with  $K = 8$  provides the best unbinding performance among the sparse  $K$ -compositional bindings. Below, we denote this  $K = 8$  solution of Eq. 30 as the octonion binding, because it employs a matrix representation of the octonions.

The octonion binding solution we constructed is not the same with the numerically optimized one, in a sense that only one of the block diagonal components is non-zero, while all block diagonal components are non-zero in the numerically optimized matrices (Figs. 3C and D). However, we found that the error of the sparse  $K$ -compositional binding is conserved under a transformation with any orthogonal matrix, which makes all block diagonal components non-zero (Appendix B.3). This result suggests that the numerically optimized solutions are consistent with the octonion binding. Note that, unlike  $K$ -compositional bindings with  $K \leq 8$ , HRR does not satisfy Eqs. 20 and 21 at a finite  $N$  (see Appendix C.1).

A binding operator  $P$  derived by minimizing  $\ell_a$  shrinks the amplitude of the signal in the reconstructed vector  $\hat{\mathbf{a}}_1$  as shown in Eq. 29 ( $\langle \hat{\mathbf{a}} \rangle_{p(b)} = \frac{2}{3} \mathbf{a}$  under the quaternion binding), meaning that the decoding is biased. However, it might be desirable to use an unbiased binding operator, which keeps the signal amplitude in the decoded vector  $\hat{\mathbf{a}}_1$  the same with the original signal  $\mathbf{a}_1$  (i.e.,  $\langle \hat{\mathbf{a}}_1 - \mathbf{a}_1 \rangle = 0$ ). Taking the expectation over  $\mathbf{b}$ , the reconstructed vector  $\hat{a}_i^1$  (Eq. 5) on average satisfies

$$\langle \hat{a}_i^1 \rangle_{p(b)} = \sum_{j=1}^N \sum_{l=1}^N \left( \sum_{k=1}^N Q_{ijk} P_{ljk} \right) a_l^1. \quad (33)$$

Thus, in order to keep the reconstructed signal amplitude the same with the original signal, under  $P = Q$ ,  $P$  should be normalized as

$$\sum_{j=1}^N \sum_{k=1}^N P_{ijk}^2 = 1, \quad (34)$$

for  $i = 1, 2, \dots, N$ . Under this normalization, the unbinding error tends to be larger, but the relative performance of various binding methods is preserved (Fig. 4C vs. Fig. 4A). In particular, the sparse  $K$ -compositional bindings with  $K = 4$  and 8 still outperform HRR with the same unbiased normalization (orange and purple lines vs. blue line in Fig. 4C).

To gain further insights into the space of the quadratic binding mechanisms, we next study the stability of the quaternion and the octonion bindings (Eq. 30 with  $K = 4$  and 8, respectively) against a perturbation. If we initialize  $P, Q, R$  as the quaternion binding plus a small random perturbation, then run the iterative optimization

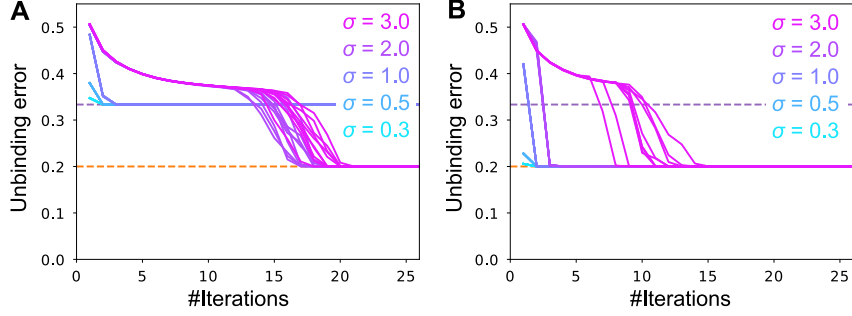


Figure 5: Local stability of the quaternion and the octonion bindings at  $N = 48$  and  $L = 1$ . **A)** Learning curve from the quaternion binding ( $K = 4$ ) plus perturbation. We constructed the initial  $P, Q, R$  by adding random Gaussian noise with the standard deviation  $\sigma/N$  to the sparse-quaternions binding. **B)** Learning curve from the octonion binding ( $K = 8$ ) plus perturbation. Both in **A** and **B**, we measure the unbinding error by  $\ell_a$ .

process (Algorithm 1), the error converges to  $1/3$ , the original error level under the quaternion binding (blue lines in Fig. 5A). On the other hand, under a large perturbation, the error instead converges to  $1/5$ , the error level under the octonion binding (purple and pink lines). These results indicate that the quaternion binding is a local minimum in the space of binding operators. The octonion binding is, on the contrary, stable against perturbation (Fig. 5B), although  $P, Q, R$  converge to different tensors when a large perturbation is added. This result suggests that the octonion binding has a large basin of attraction in the parameter space, though it only indicates a local optimality of the octonion binding, not a global one.

## 4 The binding solutions under $L > 1$

Our theoretical and numerical analyses in the previous section suggest that a binding method based on a matrix representation of octonions, the octonion binding, outperforms HRR binding under  $L = 1$ . How does this method scale to an unbinding from a composition  $\mathbf{c}$  that consists of multiple bound pairs ( $L > 1$ )?

The numerical optimization method (Algorithm 1) can be straightforwardly applied to  $L > 1$ . For instance, an update of  $P$  with respect to loss  $\ell_a$  is done by  $\text{Vec}[P_l] = (\Gamma^{q,L})^{-1} \text{Vec}[Q_l]$ , where  $N^2 \times N^2$  matrix  $\Gamma^{q,L}$  is defined as (see Appendix A.2),

$$\Gamma_{[jN+k],[mN+n]}^{q,L} \equiv \sum_i \left( \delta_{jm} L \sum_{\beta} Q_{i\beta k} Q_{i\beta n} + Q_{ijk} Q_{imn} + Q_{ijn} Q_{imk} \right). \quad (35)$$

Applying this numerical optimization to the case when  $L = 3$ , we found  $8 \times 8$  block diagonal structures in the converged binding matrices as before (Figs. 6B and C). The decoding performance of the obtained binding is better than HRR (black vs. gray dashed lines in Fig. 6A), though the relative advantage was smaller compared to the case when  $L = 1$  (Fig. 6A vs. Fig. 2A). Moreover, the octonion binding satisfies the fixed-point condition for both  $\ell_a$  and  $\ell_b$  even when  $L > 1$  (see Appendix B.3). These results indicate that the octonion binding may have an edge even when  $L > 1$ . However, it is only suggestive because both the octonion and HRR bindings perform poorly when we directly apply them to  $L > 1$  (Fig. 6A; noise-to-signal ratio is above 0.7 for both).

Below, we first show that the performance of all unbiased quadratic binding operators is lower bounded by  $\ell_a \geq \frac{NL}{N_c} + \mathcal{O}(1)$  under a mild condition, hence equi-sized binding operators (i.e.,  $N_c = N$ ), such as HRR or the octonion binding, inevitably scale poorly under  $L > 1$ . To overcome this problem, we consider two extensions: decoding with a dictionary (Plate, 1995; Smolensky et al., 2014) and decoding from a composition  $\mathbf{c}$  larger than the size of elements  $\mathbf{a}$  and  $\mathbf{b}$  ( $N_c > N$ ) (Smolensky, 1990; Frady et al., 2020). We show that under both extensions, the proposed octonion binding outperforms both HRR and a random binding under  $L \sim \mathcal{O}(1)$ , but its advantage disappears at the large  $L$  limit.

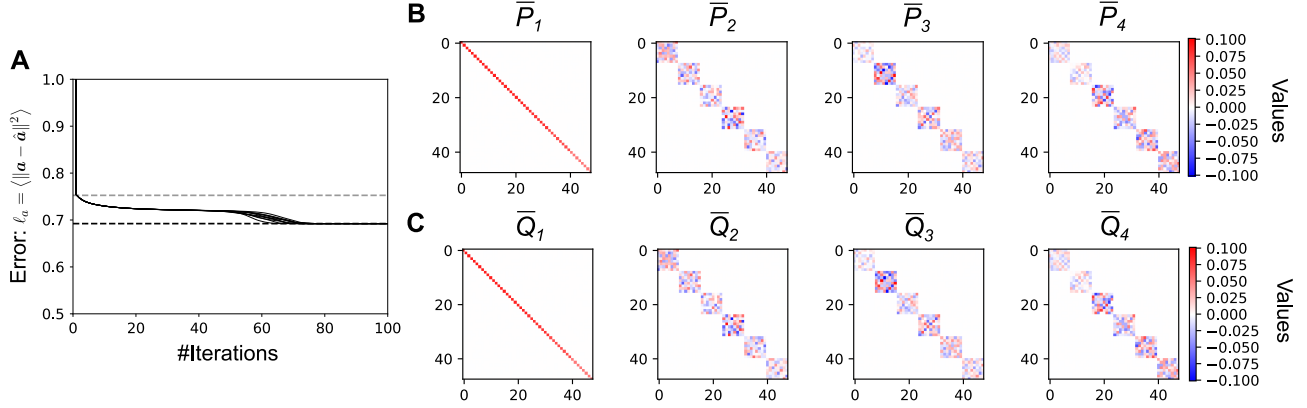


Figure 6: Numerical optimization of  $P, Q, R$  under  $N = 48, L = 3$ . **A)** Learning dynamics from ten random initializations (the same as Fig. 2A, but under  $L = 3$ ). Black and gray horizontal dashed lines are the error under the octonion binding ( $\ell = \frac{9}{13}$ ), and HRR ( $\ell = \frac{3}{4}$ ), respectively. **B, C)** Examples of the learned binding matrices after 300 iterations. The panels are the same with Figs. 3C and 3D, but calculated under  $L = 3$ . Note that  $\bar{P}_i = \bar{Q}_i$  holds for all  $i$ .

#### 4.1 Lower bound on the unbinding error

Let us first focus on the case when  $L \gg 1$ , and consider minimization of the decoding error  $\ell_a$  under a general quadratic parameterization. As we discussed previously, in order to retain the signal amplitude in the unbinding process, and thus to make the estimation unbiased, from Eq. 67,  $P$  and  $Q$  need to be normalized as

$$\sum_{j=1}^N \sum_{k=1}^{N_c} P_{ijk} Q_{ijk} = 1. \quad (36)$$

Taking the large  $L$  limit of the loss  $\ell_a$  under this constraint, as a function of  $L$ , the loss  $\ell_a$  follows (see Appendix A.3)

$$\frac{\ell_a}{L} = \frac{1}{N} \sum_{i=1}^N \sum_{l=1}^N \text{tr} [P_l Q_i^T Q_i P_l^T] + \mathcal{O}\left(\frac{1}{L}\right). \quad (37)$$

Thus, at  $L \gg 1$ , minimization of the loss  $\ell_a$  under the signal amplitude constraint is reformulated as the minimization of a Lagrangian:

$$\mathcal{L}_a = \frac{1}{2} \sum_{i=1}^N \sum_{l=1}^N \text{tr} [P_l Q_i^T Q_i P_l^T] - \sum_{i=1}^N \lambda_i (\text{tr} [P_i Q_i^T] - 1). \quad (38)$$

Solving this Lagrangian under an assumption that  $\sum_i P_i P_i^T$  is invertible, and applying Jensen's inequality, the lower bound of  $\ell_a$  is given as

$$\frac{\ell_a}{L} \geq \frac{N}{N_c} + \mathcal{O}\left(\frac{1}{L}\right), \quad (39)$$

where, recall that,  $N \equiv \dim(\mathbf{a}) = \dim(\mathbf{b})$ , and  $N_c \equiv \dim(\mathbf{c})$ . This means that the error under any quadratic bindings satisfying the invertibility condition is lower bounded by  $\ell_a \geq \frac{NL}{N_c} + C$ , where  $C$  is a term that does not depend on  $L$ . In particular, under an equi-sized composition ( $N_c = N$ ), the error is bounded by  $\ell_a \geq L + C$ .

Figure 7 describes the unbinding error  $\ell_a$  as a function of the number of bound pairs  $L$  under  $N_c = N$  for three different binding mechanisms. Under the octonion binding, the error follows  $\ell_a = L - \frac{3}{4}$  (orange line in Fig. 7), whereas under HRR,  $\ell_a = L + \frac{2}{N}$  (blue line). It means that, both binding methods tightly follow the lower bound (Eq. 39) though the octonion binding has a smaller intercept  $C$  than HRR. On the contrary, the sum binding

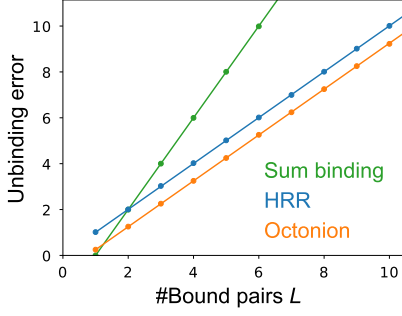


Figure 7: Comparison of the loss  $\ell_a$  under the octonion, HRR, and the sum bindings at  $N_c = N = 128$  for various  $L$ . Points are simulations and lines are theory ( $\ell_a = 2L - 1$ ,  $L + \frac{2}{N}$ , and  $L - \frac{3}{4}$  for the sum-binding, HRR, and the octonion, respectively).

( $\mathbf{c} = \sum_{\mu} (\mathbf{a}_{\mu} + \mathbf{b}_{\mu})$  and  $\hat{\mathbf{a}}_1 = \mathbf{c} - \mathbf{b}_1$ ) yields  $\ell_a = 2L - 1$  (green line in Fig. 7). Thus, it performs progressively worse compared to the two other methods as  $L$  becomes larger, though it has the smallest error under  $L = 1$ . Notably, all three methods yield errors larger than one for  $L > 1$ , meaning that the signal-to-noise ratio is smaller than one. Therefore, we need to modify these methods to perform decoding from a composition of multiple pairs. Below, we first consider decoding with a help of a dictionary, then study binding with an expanded composition ( $N_c > N$ ).

## 4.2 Decoding with a dictionary

Previous studies showed that if the system knows the dictionary from which vectors  $\{\mathbf{a}_{\mu}\}_{\mu=1}^L$  and  $\{\mathbf{b}_{\mu}\}_{\mu=1}^L$  are sampled, accurate decoding is possible even if multiple pairs are bound together (Plate, 1995; Smolensky et al., 2014). Hence, we introduce a dictionary containing  $D$  words  $\mathcal{D} = \{\mathbf{a}_d\}_{d=1}^D$ , where each word  $\mathbf{a}_d$  is sampled from an i.i.d. Gaussian distribution  $\mathcal{N}(0, I_N)$ . With this dictionary, we conduct unbinding of  $\mathbf{a}_1$  from a composition  $\mathbf{c}$  with a query  $\mathbf{b}_1$  in the following steps:

1. Unbind  $\mathbf{a}_1$  by  $\hat{a}_i^1 = \sum_j \sum_k Q_{ijk} b_j^1 c_k$ , as before.
2. Calculate  $z_{\mu} = \hat{\mathbf{a}} \cdot \mathbf{a}_{\mu}$  for all the words in the dictionary ( $\mu = 1, \dots, D$ ).
3. Pick the word  $\mathbf{a}_{\mu_o}$  with  $\mu_o \equiv \operatorname{argmax}_{\mu} z_{\mu}$ .

Note that, because all  $a_{\mu}$  have roughly the same norm ( $\|\mathbf{a}_{\mu}\|^2 \approx N$ ),  $\operatorname{argmax}_{\mu} \hat{\mathbf{a}} \cdot \mathbf{a}_{\mu}$  is equivalent to  $\operatorname{argmin}_{\mu} \|\hat{\mathbf{a}} - \mathbf{a}_{\mu}\|^2$  at the large  $N$  limit. Approximating  $p(z_1, \dots, z_D)$  with a Gaussian distribution, the probability of a misclassification is given as (see Appendix A.4)

$$P[\mu_o \neq 1] = 1 - \int \frac{dz}{\sqrt{2\pi}} \exp\left[-\frac{1}{2} \left(z - \frac{1}{\sigma_s}\right)^2\right] \left(\Phi\left[\frac{\sigma_s z}{\sigma_l}\right]\right)^{L-1} \left(\Phi\left[\frac{\sigma_s z}{\sigma_d}\right]\right)^{D-L}, \quad (40)$$

where  $\Phi[z]$  is the cumulative Gaussian distribution, and  $\sigma_s, \sigma_l, \sigma_d$  are the standard deviations of  $z_{\mu}$  under  $\mu = 1$  (the target),  $2 \leq \mu \leq L$  (the bound words), and  $L + 1 \leq \mu \leq D$  (the rest of words in the dictionary), respectively.

The standard deviations  $\sigma_s, \sigma_l$  and  $\sigma_d$  depend on the choice of the binding and unbinding methods. For instance, under the octonion binding, we get

$$\sigma_s^2 = \frac{1}{N} \left(L + \frac{3}{2}\right), \quad \sigma_l^2 = \frac{1}{N} \left(L + \frac{1}{2}\right), \quad \sigma_d^2 = \frac{1}{N} \left(L + \frac{1}{4}\right), \quad (41)$$

whereas under HRR, assuming  $N \gg 1$ ,

$$\sigma_s^2 = \frac{1}{N} (L + 3), \quad \sigma_l^2 = \frac{1}{N} (L + 2), \quad \sigma_d^2 = \frac{1}{N} (L + 1). \quad (42)$$

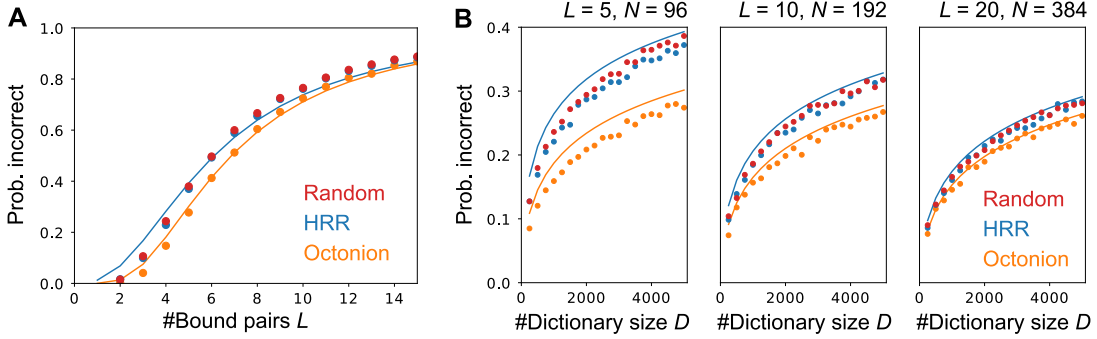


Figure 8: Decoding performance in the presence of a dictionary. **A)** Error rates (probability of incorrect classification) of the octonion, HRR and the random bindings, under various various number of bound pairs  $L$ . We set the number of the items in the dictionary to  $D = 5000$  and the vector size as  $N_c = N = 96$ . Points are simulations and lines are theory (see Appendix A.4 for the details). Analytical lines for the random binding is omitted because that is exactly the same as the line for HRR. **B)** Error rates of the octonion, HRR and the random bindings, under various dictionary sizes  $D$ . Three panels represent the errors under different  $L$  and  $N$  under a fixed ratio  $N/L$ . Points are simulations and lines are theory. The lines deviate from the points under  $L = 5$  because the Gaussianity assumption made for the theoretical lines is violated in this regime.

Therefore, we expect the classification error of two binding methods to be different under  $L \sim \mathcal{O}(1)$ , though the performance should converge to the same accuracy under  $L \gg 1$ . In particular, a small  $\sigma_s$  effectively amplifies the signal  $N/\sigma_s$ , while a small  $\sigma_s/\sigma_d$  makes a misclassification with non-bound words in the dictionary less likely (note that  $[\sigma_s/\sigma_d]_{oct} \leq [\sigma_s/\sigma_d]_{HRR}$  for  $L \geq 1$ ).

Figure 8A describes the probability of incorrect classification ( $P[\mu_o \neq 1]$ ) under the octonion binding and HRR, and also under a random binding introduced as a control. The random binding was constructed by sampling the elements of  $P$  from a Gaussian distribution  $\mathcal{N}(0, 1/N^2)$  and setting  $Q = R = P$ . As in the case of unbinding without a dictionary, the performance becomes worse as the number of bound pairs goes up (compare Fig. 8A with Fig. 7). However, even when a dozen pairs are bound to the composition, the misclassification rate is far below the chance level ( $P(\mu_o \neq 1) = 1 - \frac{1}{D}$ ) in all three binding methods. Moreover, we found that the error under the octonion binding is smaller than a random binding under a small  $L$  (orange vs. red in Fig. 8A), while that of HRR is roughly the same with the random binding (blue vs. red; some blue points are hidden under the red points).

In the comparison above, all three methods perform worse when a large number of pairs are bound to the composition, making the comparison difficult in this regime. To clarify the issue, using the fact that the signal-to-noise ratio roughly scales with  $N/L$  (Eqs. 41 and 42), we plotted the misclassification probability for different  $L$  while scaling the vector size as  $N \propto L$  (Fig. 8B). In this parameterization, the octonion binding exhibits similar error curves as a function of the dictionary size  $D$  regardless of  $L$  (orange lines). On the contrary, HRR and the random binding show higher errors under  $L = 5$  and  $L = 10$  (orange vs. blue and red points in Fig. 8B left and middle panels), though their performance converges to that of the octonion binding under  $L = 20$  (right panel). This result suggests that the performance of HRR and the random binding are suboptimal under  $L \sim \mathcal{O}(1)$ , while all three methods perform similarly under a large  $L$ .

Because the number of things humans can keep in the working memory is suggested to be less than ten (Miller, 1956; Cowan, 2001), in a cognitive process that requires binding in the working memory such as scene understanding, we expect  $L \leq 10$  to be the biologically relevant parameter regime. Our result indicates that the octonion binding outperforms HRR and the random binding in this regime, though its advantage goes away under a large  $L$ .

### 4.3 Extension of the sparse octonion binding and HRR to $N_c > N$

Even if the brain does not know the dictionary from which words are sampled, it can achieve a good decoding performance with an expansion of the composition layer. Indeed, Eq. 39 indicates that, if the size of composition

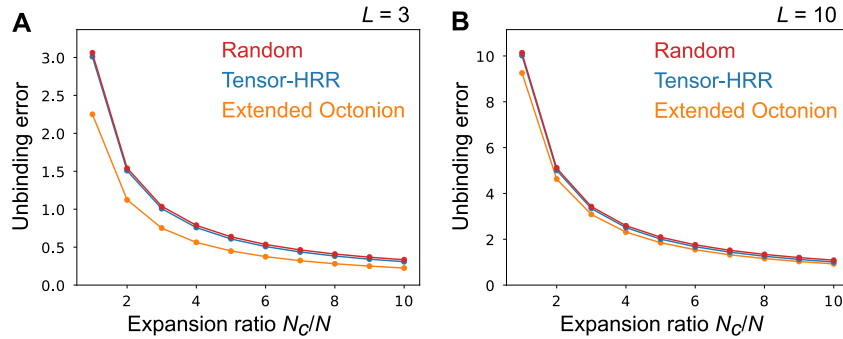


Figure 9: Comparison of the random, tensor-HRR, and the extended octonion bindings under various expansion ratios  $N_c/N$  at  $L = 3$  (A) and  $L = 10$  (B). We set  $N = 128$ . Points are simulation results, and lines are theoretical results from Eqs. 125 (extended octonions), 145 (tensor-HRR), and 101 (random).

$N_c$  scales with the (maximum) number of bound pairs  $L$ , the system can reliably perform an unbinding from a composition of multiple pairs. Thus, we next consider an extension of the octonion, HRR, and random binding mechanisms to  $N_c > N$ .

When  $N_c$  is a multiple of  $N$  but smaller than  $N^2/8$ , the octonion binding is straightforwardly extended to  $N_c > N$  by adding shifted block-diagonal components (see Appendix B.4). Under this extended octonion binding mechanism, the decoding error becomes  $\ell_a = \frac{N}{N_c} (L - 1 + \frac{2}{K})$  (orange lines in Figs. 9A and B). Notably, the leading term of  $\ell_a$  with respect to  $L$  is still the same with the lower bound (Eq. 39).

HRR can also be extended to  $N_c > N$  by considering an interpolation of HRR and the tensor product representation (Smolensky, 1990). Because the binding tensor  $P$  is given as  $P_{ijk} = \frac{1}{\sqrt{N}} \delta_{[i+j]_N, k}$  for HRR and  $P_{ijk} = \frac{1}{\sqrt{N}} \delta_{(iN+j), k}$  for the tensor product representation, we can interpolate these two bindings by setting  $P_{ijk} = \frac{1}{\sqrt{N}} \delta_{[id+j]_{dN}, k}$  for  $N_c = dN$  (see Appendix C.3). The decoding error approximately follows  $\ell_a \approx \frac{NL}{N_c} + \frac{1}{N}$  under this tensor-HRR binding (blue lines in Figs. 9A and B, partially occluded by the red lines).

Lastly, an extension of the random binding is done straightforwardly by sampling the elements of  $P$  from a Gaussian distribution with the mean zero and the variance  $1/(NN_c)$ , while setting  $Q = R = P$ . Under this method, assuming  $N, N_c \gg 1$ , the decoding error becomes (see Appendix A.6),

$$\ell_a = \frac{LN}{N_c} \left( 1 + \frac{N_c}{N^2} \right). \quad (43)$$

Thus, at  $N_c \ll N^2$ , the leading order term of the error follows the lower bound  $LN/N_c$  (red lines in Figs. 9A and B) while at  $N_c \rightarrow N^2$  limit, the error of this random binding becomes the double of the lower bound.

Because it has a small intercept, the extended octonion binding outperforms both tensor-HRR interpolation and the random binding under  $L \sim \mathcal{O}(1)$  (Fig. 9A; here  $L = 3$ ). This result again indicates that the octonion-based binding method is preferable in the parameter regime relevant to working memory-based cognitive processes. However, at  $L \gg 1$ , the random binding is as good as the extended octonion bindings (Fig. 9B;  $L = 10$ ). In fact, comparing the lower bound (Eq. 39) with Eq. 43, we can conclude that there is no quadratic binding method with invertible  $\sum_i P_i P_i^T$  that significantly outperforms the random binding when  $L \gg 1$  and  $N_c \ll N^2$ .

## 5 Discussion

In this work, we investigated optimal methods for pair-wise binding based on the VSA framework (Smolensky, 1990; Plate, 1995; Gayler, 2004). We first numerically optimized the binding and unbinding operators for the best unbinding performance assuming only one pair is bound to the composition vector. We found that the numerically optimized binding operators outperform HRR, a popular method for binding (Fig. 2). Moreover, we revealed that

there is a hidden  $8 \times 8$  block structure in the optimized binding and unbinding matrices (Fig. 3). By analytically deriving a sufficient condition for a fixed-point of the loss function, we show that the  $8 \times 8$  block structure is originated from a matrix representation of the octonion algebra, an eight-dimensional extension of the complex numbers (Fig. 4). Furthermore, we showed that even when several pairs are bound into a composition, the proposed binding method based on the octonion outperforms previously proposed methods both under the dictionary decoding (Fig. 8) and unbinding from an expanded composition (Fig. 9). When there are many bound pairs in a composition, however, the advantage of the proposed method vanishes, and even a random binding shows approximately the optimal unbinding performance under a mild condition (Figs. 8 and 9).

We introduced two key assumptions for deriving these conclusions: Both binding and unbinding operators have quadratic forms, and input vectors are i.i.d. random Gaussian vectors. The former assumption is reasonable under the latter assumption because a quadratic binding should be enough to capture the statistical relationship between the inputs when the inputs are Gaussian. We leave an investigation of the optimal binding under general input statistics for future works.

Many binding mechanisms have been proposed previously in the framework of VSA (Smolensky, 1990; Plate, 1995; Kanerva et al., 1997; Gallant and Okaywe, 2013; Gosmann and Eliasmith, 2019; Frady et al., 2020). In particular, Frady and colleagues proposed a block-wise circular convolution method to conserve the sparsity of the composition (Frady et al., 2020). At the limit where each block is  $2 \times 2$  matrix, their binding method corresponds to our sparse  $K$ -compositional binding with  $K = 2$  in which a matrix representation of the complex numbers is used for binding. However, their analysis is limited to the case when the input is a block-wise one-hot vector, and they did not investigate other block-wise binding mechanisms. In addition, the relationship between the Clifford algebra, a generalization of the quaternion algebra, and HRR was previously investigated by Aerts and colleagues (Aerts et al., 2009). However, they did not study the space of binding mechanisms or the optimization of binding methods.

Recent experimental results found a mixed representation of sensory stimuli and context cues in the prefrontal cortex (Rigotti et al., 2013) and hippocampus (Nieh et al., 2021). However, it remains unclear whether mixed representation in the brain is random or structured (Hirokawa et al., 2019). Our results suggest that depending on the task configuration, random binding might be enough for an accurate unbinding, though it is unclear if unbinding is crucial in the tasks employed in these experiments.

The binding problem is also an important topic in machine learning (Greff et al., 2020). In knowledge graph embedding tasks (Nickel et al., 2015), Nickel and colleagues showed that HRR yields a better generalization performance than methods based on nonlinear-projection of a concatenated vector (Nickel et al., 2016). Moreover, in visual question answering tasks, binding of an image representation and a query representation is crucial for solving the task. The Hadamard product is often employed for this binding (Antol et al., 2015; Santoro et al., 2017), but more elaborate binding mechanisms, such as self-attention on concatenated vectors, are suggested to improve the learning performance (Teney et al., 2018).

Lastly, unlike the quaternions, the octonions are rarely applied to the domain of science (Baez, 2002). Our work provides a rare practical application of octonion algebra. More generally, our work indicates a potential link between the mathematics of quadratic forms and the binding problem in cognitive science and machine learning.

# Appendix

## A Quadratic binding

### A.1 Fixed-point condition of the mean-squared error

From Eqs. 4, 5, and 7, the loss function  $\ell_a$  is written as

$$\begin{aligned}\ell_a &= \frac{1}{N} \left\langle \sum_{i=1}^N (a_i^1 - \hat{a}_i^1)^2 \right\rangle_{p(S)} \\ &= \frac{1}{N} \left\langle \sum_{i=1}^N \left( a_i^1 - \sum_{\mu=1}^L \sum_{j=1}^N \sum_{l=1}^N \sum_{m=1}^N \left[ \sum_{k=1}^{N_c} Q_{ijk} P_{lmk} \right] b_j^1 b_m^\mu a_l^\mu \right)^2 \right\rangle_{p(S)}\end{aligned}\quad (44)$$

where  $\langle \cdot \rangle_{p(S)}$  is the expectation over random vectors  $\mathbf{a}_\mu$  and  $\mathbf{b}_\mu$  sampled i.i.d. from a Gaussian distribution  $N(\mathbf{0}, I_N)$ . For simplicity, let us introduce a fourth-order tensor  $M$  as,

$$M_{mj}^{li} \equiv \sum_{k=1}^{N_c} Q_{ijk} P_{lmk}. \quad (45)$$

Then the loss is rewritten as

$$\ell_a = \frac{1}{N} \left\langle \sum_{i=1}^N \left( (a_i^1)^2 - 2 \sum_{\mu=1}^L \sum_{j=1}^N \sum_{l=1}^N \sum_{m=1}^N M_{mj}^{li} a_i^1 a_l^\mu b_j^1 b_m^\mu + \left( \sum_{\mu=1}^L \sum_{j=1}^N \sum_{l=1}^N \sum_{m=1}^N M_{mj}^{li} a_l^\mu b_j^1 b_m^\mu \right)^2 \right) \right\rangle_{p(S)} \quad (46)$$

The expectation over the last quadratic term becomes

$$\begin{aligned}& \left\langle \sum_{i=1}^N \left( \sum_{\mu=1}^L \sum_{j=1}^N \sum_{l=1}^N \sum_{m=1}^N M_{mj}^{li} a_l^\mu b_j^1 b_m^\mu \right)^2 \right\rangle \\ &= \sum_{\mu=2}^L \sum_i \sum_l \sum_j \sum_m (M_{mj}^{li})^2 + \sum_i \sum_l \left( \sum_j \sum_m M_{mj}^{li} M_{mj}^{li} + \sum_j \sum_m M_{mj}^{li} M_{jm}^{li} + \sum_j \sum_m M_{jj}^{li} M_{mm}^{li} \right) \\ &= \sum_i \sum_l \left( \left( \sum_j M_{jj}^{li} \right)^2 + \sum_j \sum_m M_{mj}^{li} [L \cdot M_{mj}^{li} + M_{jm}^{li}] \right),\end{aligned}\quad (47)$$

where summation runs from 1 to  $N$  unless otherwise stated. In the second line, we used

$$\langle b_i^1 b_j^1 b_k^1 b_l^1 \rangle = \delta_{ij} \delta_{kl} + \delta_{ik} \delta_{jl} + \delta_{il} \delta_{jk}. \quad (48)$$

Thus, the loss  $\ell_a$  is written as

$$\ell_a = 1 - \frac{2}{N} \sum_i \sum_j M_{jj}^{ii} + \frac{1}{N} \sum_i \sum_l \left( \left( \sum_j M_{jj}^{li} \right)^2 + \sum_j \sum_m M_{mj}^{li} [L \cdot M_{mj}^{li} + M_{jm}^{li}] \right), \quad (49)$$

Using  $P$  and  $Q$  instead of  $M$  via Eq. 45, this equation is also written as

$$\ell_a = 1 - \frac{2}{N} \sum_i \text{tr} [P_i Q_i^T] + \frac{1}{N} \sum_i \sum_l \left( (\text{tr} [P_l Q_i^T])^2 + \text{tr} [P_l Q_i^T (L \cdot Q_i P_l^T + P_l Q_i^T)] \right). \quad (50)$$



Here we defined  $N \times N$  matrices  $\{P_i\}_{i=1}^N$  and  $\{Q_i\}_{i=1}^N$  by  $[P_i]_{jk} = P_{ijk}$  and  $[Q_i]_{jk} = Q_{ijk}$  as in the main text. By taking the gradient with respect to  $P_l$  and  $Q_i$ , we get

$$\begin{aligned}\frac{\partial \ell_a}{\partial P_l} = 0 &\Leftrightarrow Q_l = \sum_i (tr [P_l Q_i^T] I_N + L \cdot P_l Q_i^T + Q_i P_l^T) Q_i, \\ \frac{\partial \ell_a}{\partial Q_i} = 0 &\Leftrightarrow P_i = \sum_l (tr [P_l Q_i^T] I_N + L \cdot Q_i P_l^T + P_l Q_i^T) P_l,\end{aligned}\tag{51}$$

where  $I_N$  is the size  $N$  identity matrix. Under  $P = Q$  constraint, the above equations are rewritten as

$$P_i = \sum_l (tr [P_l P_i^T] I_N + L \cdot P_i P_l^T + P_l P_i^T) P_l.\tag{52}$$

On the other hand, as a function of  $\{P_i\}$  and  $\{R_i\}$ , the decoding error for  $\mathbf{b}$  is given as

$$\ell_b = 1 - \frac{2}{N} \sum_i tr [P_i R_i^T] + \frac{1}{N} \sum_i \sum_l (tr [P_i R_i^T R_l P_l^T] + tr [P_l R_i^T (L \cdot R_i P_l^T + R_l P_i^T)]).\tag{53}$$

Taking the gradient with respect to  $P$  and  $R$ , we get

$$\begin{aligned}\frac{\partial \ell_b}{\partial P_l} = 0 &\Leftrightarrow R_l = \sum_i (L \cdot P_l R_i^T R_i + P_i [R_i^T R_l + R_l^T R_i]), \\ \frac{\partial \ell_b}{\partial R_i} = 0 &\Leftrightarrow P_i = \sum_l (L \cdot R_i P_l^T P_l + R_l [P_l^T P_i + P_i^T P_l]).\end{aligned}\tag{54}$$

In particular, under  $P = R$  constraint, the fixed-point condition on  $\{P_i\}$  with respect to  $\ell_b$  is given as

$$P_i = \sum_l (L \cdot P_i P_l^T P_l + P_l P_i^T P_l + P_l P_l^T P_i),\tag{55}$$

for  $i = 1, \dots, N$ .

## A.2 Details of the numerical optimization algorithm

Rewriting the fixed-point condition of  $P_l$  with respect to the loss  $\ell_a$  (Eq. 51), we get

$$Q_{ljk} = \sum_m \sum_n \sum_i \left( \delta_{jm} L \sum_\beta Q_{i\beta k} Q_{i\beta n} + Q_{ijk} Q_{imn} + Q_{ijn} Q_{imk} \right) P_{lmn},\tag{56}$$

for  $j, k = 1, \dots, N$ . Thus, introducing an  $N^2 \times N^2$  matrix  $\Gamma^q$  by

$$\Gamma_{[jN+k],[mN+n]}^q \equiv \sum_i \left( \delta_{jm} L \sum_\beta Q_{i\beta k} Q_{i\beta n} + Q_{ijk} Q_{imn} + Q_{ijn} Q_{imk} \right),\tag{57}$$

we get  $Q_{ljk} = \sum_{m,n} \Gamma_{[jN+k],[mN+n]}^q P_{lmn}$ . Therefore, we can derive the binding tensor  $P$  that minimizes the loss  $\ell_a$  under a fixed  $Q$  by solving this linear equation as

$$\text{Vec}[P_l] = (\Gamma^q)^{-1} \text{Vec}[Q_l],\tag{58}$$

where  $\text{Vec}[P_l]$  and  $\text{Vec}[Q_l]$  are the vector representations of  $N \times N$  matrices  $P_l$  and  $Q_l$ , respectively. From a similar calculation, the unbinding tensor  $Q$  that minimizes the loss  $\ell_a$  under a fixed  $P$  is given by

$$\text{Vec}[Q_l] = (\Gamma^{pa})^{-1} \text{Vec}[P_l],\tag{59}$$

where  $\Gamma^{pa}$  is an  $N^2 \times N^2$  matrix:

$$\Gamma_{[jN+k],[mN+n]}^{pa} \equiv \sum_i \left( \delta_{jm} L \sum_{\beta} P_{i\beta k} P_{i\beta n} + P_{ijk} P_{imn} + P_{ijn} P_{imk} \right). \quad (60)$$

To consider minimization of  $\ell_b$ , we rewrite the fixed-point condition of  $P_i$  with respect to  $\ell_b$  (Eq. 54) as

$$R_{lmk} = \sum_i \sum_n \Gamma_{lkin}^r P_{imn}, \quad (61)$$

where

$$\Gamma_{[lN+k],[iN+n]}^r \equiv \delta_{il} L \sum_{\alpha} \sum_j R_{\alpha j n} R_{\alpha j k} + \sum_j R_{ljk} R_{ijn} + \sum_j R_{ljn} R_{ijk} \quad (62)$$

is an  $N^2 \times N^2$  matrix. Let us construct  $N \times N$  matrices  $\check{R}_m$  and  $\check{P}_m$  by  $[\check{R}_m]_{l,k} = R_{lmk}$  and  $[\check{P}_m]_{l,k} = P_{lmk}$  respectively (for  $m = 1, \dots, N$ ). Then, for a given  $R$ , the tensor  $P$  that satisfies the fixed-point condition of  $\ell_b$  is derived as

$$\text{Vec} [\check{P}_m] = (\Gamma^r)^{-1} \text{Vec} [\check{R}_m] \quad (63)$$

for  $m = 1, \dots, N$ . Similarly, the fixed-point condition for  $R$  is written as

$$P_{ijk} = \sum_l \sum_n \Gamma_{ikln}^{pb} R_{ljn} \quad (64)$$

where

$$\Gamma_{[iN+k],[lN+n]}^{pb} \equiv \delta_{il} L \sum_{\alpha} \sum_m P_{\alpha mk} P_{\alpha mn} + \sum_m P_{imk} P_{lmn} + \sum_m P_{imn} P_{lmk}. \quad (65)$$

Therefore, for a given  $P$ ,  $R$  should satisfy

$$\text{Vec} [\check{R}_j] = (\Gamma^{pb})^{-1} \text{Vec} [\check{P}_j] \quad (66)$$

for  $j = 1, \dots, N$ .

Combining the fixed-point algorithms for  $P, Q$  in the main text, and for  $P, R$  described above, we obtain an iterative optimization algorithm of  $P, Q, R$ . In a pseudocode, this algorithm is written as Algorithm 1. In Figures 2 and 3, we initialized  $P, Q, R$  randomly by setting their elements from i.i.d Gaussian with variance  $\frac{1}{NN_c}$ , then performed Algorithm 1 for  $T = 100$  iterations under  $L = 1$ . In Figure 5, we instead initialized  $P, Q, R$  as a sparse  $K$ -compositional binding tensor plus an element-wise Gaussian perturbation with variance  $\sigma^2/N^2$ . Noise was added to  $P, Q, R$  independently (hence  $P \neq Q \neq R$  after the perturbation). Figure 6 describes the optimization process under  $L = 3$ . The optimization process becomes slower and the advantage over HRR gets smaller (compare Fig. 6A with Fig. 2A). However, the obtained binding matrices exhibit  $8 \times 8$  block diagonal structures when projected to the space where  $\bar{P}_1$  is diagonal (Figs. 6B and C).

### A.3 Lower bound on the cardinality dependence

Taking the expectation over  $\mathbf{b}$ , the readout (Eq. 5) becomes

$$\langle \hat{a}_i^1 \rangle_{p(\mathbf{b})} = \left\langle \sum_{\mu} \sum_j \sum_l \sum_m \left( \sum_k Q_{ijk} P_{lmk} \right) b_j^1 b_m^{\mu} a_j^{\mu} \right\rangle_{p(\mathbf{b})} = \sum_j \sum_l \left( \sum_k Q_{ijk} P_{ljk} \right) a_l^1. \quad (67)$$

Thus, in order to retain the amplitude of the signal in the readout,  $P$  and  $Q$  need to satisfy

$$\sum_{j=1}^N \sum_{k=1}^{N_c} P_{ijk} Q_{ijk} = 1. \quad (68)$$

Note that P and Q that minimize  $\ell_a$  do not necessarily satisfy this condition. However, the readout becomes unbiased against the original signal under this condition (i.e.,  $\langle \hat{a}_i^1 - a_i^1 \rangle = 0$ ). Under this constraint, Eq. 50 is rewritten as

$$\ell_a = \frac{1}{N} \sum_i \sum_{l \neq i} (tr [P_l Q_i^T])^2 + \frac{1}{N} \sum_i \sum_l tr [P_l Q_i^T (P_l Q_i^T + L Q_i P_l^T)]. \quad (69)$$

Therefore at the large  $L$  limit, the last term,  $tr [P_l Q_i^T Q_i P_l^T]$ , becomes the dominant factor of the loss function. Hence, we consider minimization of this dominant term under the constraint Eq. 68. The Lagrangian for this constrained minimization is given by

$$\mathcal{L}_a = \frac{1}{2} \sum_{i=1}^N \sum_{l=1}^N tr [P_l Q_i^T Q_i P_l^T] - \sum_{i=1}^N \lambda_i (tr [P_i Q_i^T] - 1), \quad (70)$$

where  $\lambda_i \geq 0$  is a Lagrange multiplier. The minimizer  $Q$  needs to satisfy

$$\frac{\partial \mathcal{L}_a}{\partial Q_i} = 0 \Leftrightarrow \lambda_i P_i = Q_i \sum_{l=1}^N P_l^T P_l, \quad (71)$$

for  $i = 1, \dots, N$ . Let us assume that  $\sum_{l=1}^N P_l^T P_l$  is invertible. Note that,  $\sum_{l=1}^N P_l^T P_l$  might not be invertible especially under  $N \ll N_c$ , because  $P_l$  is a  $N \times N_c$  matrix. However, because  $\sum_{l=1}^N P_l^T P_l$  is a positive semi-definite matrix, if it is not invertible, the composition  $\mathbf{c}$  spans a subspace of  $N_c$  dimensional space, which should not provide any advantage over smaller  $N_c$ . Under the invertibility assumption,  $Q_i$  should satisfy

$$Q_i = \lambda_i P_i \left( \sum_{l=1}^N P_l^T P_l \right)^{-1}. \quad (72)$$

Substituting  $Q_i$  in Eq. 68 with the equation above, we get

$$1 = tr [P_i Q_i^T] = \lambda_i tr \left[ P_i^T P_i \left( \sum_{l=1}^N P_l^T P_l \right)^{-1} \right]. \quad (73)$$

Because  $P_i \left( \sum_l P_l^T P_l \right)^{-1} P_i^T$  is a positive semi-definite matrix,  $tr \left[ P_i^T P_i \left( \sum_l P_l^T P_l \right)^{-1} \right] > 0$  (If all the eigenvalues are zero, the equation above does not hold). Thus,

$$\lambda_i = \left( tr \left[ P_i^T P_i \left( \sum_{l=1}^N P_l^T P_l \right)^{-1} \right] \right)^{-1}. \quad (74)$$

Multiplying Eq. 71 with  $Q_i^T$  from the right, taking the trace, and summing over  $i$ ,

$$\sum_{i=1}^N \lambda_i tr [P_i Q_i^T] = \sum_{i=1}^N tr \left[ Q_i^T Q_i \sum_{l=1}^N P_l^T P_l \right]. \quad (75)$$

Therefore,

$$\begin{aligned} \sum_{i=1}^N \sum_{l=1}^N tr [P_l Q_i^T Q_i P_l^T] &= \sum_{i=1}^N \lambda_i \\ &= \sum_{i=1}^N \left( tr \left[ P_i^T P_i \left( \sum_{l=1}^N P_l^T P_l \right)^{-1} \right] \right)^{-1} \\ &\geq \frac{N^2}{\sum_{i=1}^N tr \left[ P_i^T P_i \left( \sum_{l=1}^N P_l^T P_l \right)^{-1} \right]} = \frac{N^2}{N_c}. \end{aligned} \quad (76)$$

In the last line, we used Jensen's inequality with  $1/x$  (i.e.  $(\frac{1}{N} \sum_i x_i)^{-1} \leq \frac{1}{N} \sum_i \frac{1}{x_i}$ ). Therefore, as long as  $\sum_{l=1}^N P_l^T P_l$  is invertible, the dominant error term of  $\ell_a$  is lower bounded by  $LN/N_c$ .

## A.4 Decoding with a dictionary

Although decoding in vector symbolic architecture is typically noisy especially when  $L > N_c/N$ , if we know the dictionary of vectors from which  $\mathbf{a}$  is sampled, it is possible to recover  $\mathbf{a}$  accurately by matching the decoded vector  $\hat{\mathbf{a}}$  with vectors  $\{\mathbf{a}_\mu\}_{\mu=1}^D$  in the dictionary. Below, we set  $\mu = 1$  as the target vector (as before),  $\mu = 2, \dots, L$  as the other vectors bound to the composition  $\mathbf{c}$ , and  $\mu = L + 1, \dots, D$  as the rest of vectors in the dictionary. We denote the inner product between the retrieved vector  $\hat{\mathbf{a}}_1$  and  $\mu$ -th vector in the dictionary  $\mathbf{a}_\mu$  as

$$z_\mu \equiv \hat{\mathbf{a}}_1^T \mathbf{a}_\mu, \quad (77)$$

then pick  $\mathbf{a}_\mu$  with the largest  $z_\mu$  as the decoded vector. Because all  $\mathbf{a}_\mu$  has nearly the same norm ( $\|\mathbf{a}_\mu\|^2 \approx N$ ), this is approximately equivalent to choosing  $\mathbf{a}_\mu$  closest to  $\hat{\mathbf{a}}_1$  in term of L2-norm (i.e.,  $\operatorname{argmin}_\mu \|\hat{\mathbf{a}}_1 - \mathbf{a}_\mu\|^2$ ). The probability of a correct classification under this decoding method is

$$P_{\text{correct}} = \int dz_1 \dots dz_D P[z_1, \dots, z_D] \hat{\theta}[z_1 > z_2, \dots, z_1 > z_D], \quad (78)$$

where  $\hat{\theta}[x]$  is the indicator function. Because  $\{z_\mu\}$  are not independent with each other,  $P_{\text{correct}}$  is generally not analytically tractable. However, we can approximately estimate  $P_{\text{correct}}$  under  $N \gg 1$  for any quadratic binding methods satisfying Eq. 68 in a similar manner to previous works (Murdock, 1982; Plate, 1995; Steinberg and Sompolinsky, 2022). We first normalize variables  $\{z_\mu\}_{\mu=1}^D$  as

$$\hat{z}_\mu \equiv \frac{\hat{\mathbf{a}}_1^T \mathbf{a}_\mu}{\mathbf{a}_1^T \mathbf{a}_1}. \quad (79)$$

This normalization improves the accuracy of the Gaussian approximation we introduce below. Because the normalization does not change the relative order among  $\{z_\mu\}_{\mu=1}^D$ , the probability of a correct classification is written as

$$P_{\text{correct}} = \int d\hat{z}_1 \dots d\hat{z}_D P[\hat{z}_1, \dots, \hat{z}_D] \hat{\theta}[\hat{z}_1 > \hat{z}_2, \dots, \hat{z}_1 > \hat{z}_D] \quad (80)$$

To evaluate this integral, we approximate the probability distribution  $P[\hat{z}_1, \dots, \hat{z}_D]$  with a Gaussian distribution:

$$P[\hat{z}_1, \dots, \hat{z}_D] \approx q[\hat{z}_1, \dots, \hat{z}_D] \equiv N(\mathbf{z}; \bar{\mathbf{z}}, \Sigma), \quad (81)$$

where  $\mathbf{z} = [\hat{z}_1, \dots, \hat{z}_D]^T$ . By definition,  $\hat{z}_\mu$  follows

$$\hat{z}_\mu = \frac{1}{\sum_{k=1}^N (a_k^1)^2} \sum_{\nu=1}^L \sum_{i=1}^N \sum_{j=1}^N \sum_{l=1}^N \sum_{m=1}^N M_{mj}^{li} a_i^\mu a_l^\nu b_j^1 b_m^\nu, \quad (82)$$

where  $M_{mj}^{li} \equiv \sum_k P_{mk} Q_{ijk}$  (Eq. 45). Taking the expectation over randomly sampled  $\{\mathbf{a}_\mu\}_{\mu=1}^D$  and  $\{\mathbf{b}_\mu\}_{\mu=1}^L$ , the mean is estimated as

$$\langle \hat{z}_\mu \rangle = \left\langle \frac{\delta_{1\mu}}{\sum_{k=1}^N (a_k^1)^2} \sum_i \sum_j M_{jj}^{ii} (a_i^1)^2 \right\rangle = \delta_{1\mu}$$

Here, we used Eq. 68. On the other hand, the covariance becomes

$$\begin{aligned} \Sigma_{\mu\nu} &= \langle (\hat{z}_\mu - \delta_{1\mu})(\hat{z}_\nu - \delta_{1\nu}) \rangle \\ &= \sum_{\rho, \sigma} \sum_{i, i'} \sum_{j, j'} \sum_{l, l'} \sum_{m, m'} M_{mj}^{li} M_{m'j'}^{l'i'} \langle b_j^1 b_m^\rho b_{j'}^1 b_{m'}^\sigma \rangle \left\langle \frac{1}{(\sum_k a_k^1 a_k^1)^2} a_i^\rho a_i^\mu a_{l'}^\sigma a_{l'}^\nu \right\rangle - \delta_{1\mu} \delta_{1\nu}, \end{aligned} \quad (83)$$

The expectation over  $\mathbf{b}$  is non-zero only when  $\rho = \sigma$ , but given  $\rho = \sigma$ , the expectation over  $\mathbf{a}$  is non-zero only when  $\mu = \nu$ . Therefore,  $\Sigma_{\mu\nu} = 0$  for  $\mu \neq \nu$ , meaning that the joint distribution  $q[\hat{z}_1, \dots, \hat{z}_D]$  is factorized under the Gaussian approximation. The second moment is evaluated as

$$\langle (\hat{z}_\mu)^2 \rangle = \sum_{\rho=1}^L \sum_{i, i'} \sum_{j, j'} \sum_{l, l'} \sum_{m, m'} M_{mj}^{li} M_{m'j'}^{l'i'} \langle b_j^1 b_{j'}^1 b_m^\rho b_{m'}^\rho \rangle \left\langle \frac{1}{(\sum_k a_k^1 a_k^1)^2} a_i^\mu a_i^\mu a_{l'}^\rho a_{l'}^\rho \right\rangle. \quad (84)$$

The expectation over  $\mathbf{b}$  is given as

$$\langle b_j^1 b_{j'}^1 b_m^\rho b_{m'}^\rho \rangle = \delta_{jj'} \delta_{mm'} + \delta_{1\rho} [\delta_{jm} \delta_{j'm'} + \delta_{jm'} \delta_{j'm}], \quad (85)$$

while the expectation over  $\mathbf{a}$  is estimated as (see Appendix A.5)

$$\left\langle \frac{1}{(\sum_k a_k^1 a_k^1)^2} a_i^\mu a_{i'}^\mu a_l^\rho a_{l'}^\rho \right\rangle = \begin{cases} \frac{\delta_{ii'} \delta_{ll'} + \delta_{\mu\rho} (\delta_{il} \delta_{i'l'} + \delta_{i'l} \delta_{i'l'})}{(N-2)(N-4)} & \mu \geq 2 \\ \frac{\delta_{ii'} \delta_{ll'}}{N(N-2)} + \frac{\delta_{1\rho} (\delta_{il} \delta_{i'l'} + \delta_{i'l} \delta_{i'l'})}{N(N+2)} & \mu = 1. \end{cases} \quad (86)$$

Thus, for  $\mu > 2$ , the variance  $\langle (\hat{z}_\mu)^2 \rangle$  follows

$$\langle (z_\mu)^2 \rangle = \sigma_o^2 + \sigma_1^2 + [\mu \leq L]_+ \sigma_2^2, \quad (87)$$

where

$$\begin{aligned} \sigma_0^2 &\equiv \frac{1}{(N-2)(N-4)} \sum_\rho \sum_{i,i'} \sum_{j,j'} \sum_{l,l'} \sum_{m,m'} M_{mj}^{li} M_{m'j'}^{l'i'} \delta_{jj'} \delta_{mm'} \delta_{ii'} \delta_{ll'}, \\ \sigma_1^2 &\equiv \frac{1}{(N-2)(N-4)} \sum_{i,i'} \sum_{j,j'} \sum_{l,l'} \sum_{m,m'} M_{mj}^{li} M_{m'j'}^{l'i'} [\delta_{jm} \delta_{j'm'} + \delta_{jm'} \delta_{j'm}] \delta_{ii'} \delta_{ll'}, \\ \sigma_2^2 &\equiv \frac{1}{(N-2)(N-4)} \sum_{i,i'} \sum_{j,j'} \sum_{l,l'} \sum_{m,m'} M_{mj}^{li} M_{m'j'}^{l'i'} \delta_{jj'} \delta_{mm'} [\delta_{il} \delta_{i'l'} + \delta_{i'l} \delta_{i'l'}], \end{aligned} \quad (88)$$

Note that,  $\sigma_2^2$  term appears only when the vector  $\mathbf{a}_\mu$  is bound to the composition  $\mathbf{c}$  (ie,  $\mu \leq L$ ). Summing over the delta functions and using  $N \gg 1$ , the components  $\sigma_0^2$ ,  $\sigma_1^2$ ,  $\sigma_2^2$  are rewritten as

$$\begin{aligned} \sigma_0^2 &= \frac{L}{N^2} \sum_{i,l} \sum_{j,m} (M_{mj}^{li})^2, \\ \sigma_1^2 &= \frac{1}{N^2} \sum_{i,l} \left( \left[ \sum_j M_{jj}^{li} \right]^2 + \sum_{j,m} M_{mj}^{li} M_{jm}^{li} \right), \\ \sigma_2^2 &= \frac{1}{N^2} \sum_{j,m} \left( \left[ \sum_i M_{mj}^{ii} \right]^2 + \sum_{i,l} M_{mj}^{li} M_{mj}^{il} \right), \end{aligned} \quad (89)$$

On the other hand, at  $\mu = 1$ , the variance follows

$$\langle (z_\mu - \delta_{1\mu})^2 \rangle \approx \sigma_o^2 + \sigma_1^2 + \sigma_2^2 + \sigma_3^2, \quad (90)$$

where the extra term  $\sigma_3^2$  is given as

$$\begin{aligned} \sigma_3^2 &\equiv \frac{1}{N(N+2)} \sum_{i,i'} \sum_{j,j'} \sum_{l,l'} \sum_{m,m'} M_{mj}^{li} M_{m'j'}^{l'i'} (\delta_{il} \delta_{i'l'} + \delta_{i'l} \delta_{i'l'}) (\delta_{jm} \delta_{j'm'} + \delta_{jm'} \delta_{j'm}) - 1 \\ &= \frac{1}{N(N+2)} \left( \sum_{i,j} M_{jj}^{ii} \right)^2 - 1 + \frac{1}{N(N+2)} \sum_{i,i'} \sum_{j,j'} \sum_{l,l'} \sum_{m,m'} M_{mj}^{li} M_{m'j'}^{l'i'} (\delta_{il} \delta_{i'l'} \delta_{jm'} \delta_{j'm} + \delta_{i'l} \delta_{i'l'} [\delta_{jm} \delta_{j'm'} + \delta_{jm'} \delta_{j'm}]) \\ &\approx \frac{-2}{N} + \frac{1}{N^2} \left( \sum_{j,m} \left[ \sum_i M_{mj}^{ii} \right] \left[ \sum_l M_{jm}^{ll} \right] + \sum_{i,l} \left[ \sum_j M_{jj}^{li} \right] \left[ \sum_m M_{mm}^{il} \right] + \sum_{i,l} \sum_{j,m} M_{mj}^{li} M_{jm}^{il} \right). \end{aligned} \quad (91)$$

Notably, of the four terms  $\sigma_0^2, \dots, \sigma_3^2$  consist of the variance, only  $\sigma_0^2$  scales with the number of bound pairs  $L$ . Thus, at the large  $L$  limit, the variance of all  $\mu$  follows

$$\langle (\hat{z}_\mu - \delta_{1\mu})^2 \rangle = L \left( \sum_{i,l} \sum_{j,m} (M_{mj}^{li})^2 + \mathcal{O}\left(\frac{1}{L}\right) \right) \geq L \left( \frac{N^2}{N_c} + \mathcal{O}\left(\frac{1}{L}\right) \right). \quad (92)$$

The last inequality follows from Eq. 76. On the other hand, under  $L \sim \mathcal{O}(1)$ ,  $\sigma_1^2$ ,  $\sigma_2^2$ , and  $\sigma_3^2$  may play an important role. For convenience, let us denote

$$\sigma_s^2 \equiv \sigma_0^2 + \sigma_1^2 + \sigma_2^2 + \sigma_3^2, \quad \sigma_l^2 \equiv \sigma_0^2 + \sigma_1^2 + \sigma_2^2, \quad \sigma_d^2 \equiv \sigma_0^2 + \sigma_1^2. \quad (93)$$

The first term  $\sigma_s^2$  corresponds to the variance of the target readout  $\hat{z}_1$ , while  $\sigma_l^2$  is the variance of readout  $\hat{z}_\mu$  for  $\mu = 2, \dots, L$ , and  $\sigma_d^2$  is the variance of  $\hat{z}_\mu$  for  $\mu = L+1, \dots, D$ . Because  $q[\hat{z}_1, \dots, \hat{z}_D]$  is factorized, using  $\sigma_s^2, \sigma_l^2, \sigma_d^2$ , we get

$$\begin{aligned} P_{\text{correct}} &\approx \int d\hat{z}_1 q[\hat{z}_1] \prod_{\mu=2}^D \int d\hat{z}_\mu q[\hat{z}_\mu] \theta[\hat{z}_1 > \hat{z}_\mu] \\ &= \int \frac{d\hat{z}_1}{\sqrt{2\pi\sigma_s^2}} e^{-(\hat{z}_1-1)^2/2\sigma_s^2} \left( \int_{-\infty}^{\hat{z}_1} \frac{dz_l}{\sqrt{2\pi\sigma_l^2}} e^{-z_l^2/2\sigma_l^2} \right)^{L-1} \left( \int_{-\infty}^{\hat{z}_1} \frac{dz_d}{\sqrt{2\pi\sigma_d^2}} e^{-z_d^2/2\sigma_d^2} \right)^{D-L} \\ &= \int \frac{dz}{\sqrt{2\pi}} \exp\left[-\frac{1}{2}\left(z - \frac{1}{\sigma_s}\right)^2\right] \left(\Phi\left[\frac{\sigma_s z}{\sigma_l}\right]\right)^{L-1} \left(\Phi\left[\frac{\sigma_s z}{\sigma_d}\right]\right)^{D-L}, \end{aligned}$$

where  $\Phi[z] \equiv \int_{-\infty}^z \frac{dy}{\sqrt{2\pi}} e^{-y^2/2}$  is the cumulative distribution function of a Gaussian distribution  $\mathcal{N}(0, 1)$ . Here,  $\left(\Phi\left[\frac{\sigma_s z}{\sigma_l}\right]\right)^{L-1}$  evaluates the probability of correct classification against vectors in the composition  $\mathbf{c}$ , while  $\left(\Phi\left[\frac{\sigma_s z}{\sigma_d}\right]\right)^{D-L}$  captures the classification accuracy against the rest of words in the dictionary.

Because  $\sigma_s^2, \sigma_l^2, \sigma_d^2$  depend on the choice of the binding and unbinding operators  $P$  and  $Q$ ,  $P_{\text{correct}}$  also depends on the binding methods. For instance, under the octonion binding, from Eq. 89 and Eq. 30, we get

$$\sigma_s^2 = \frac{1}{N} \left(L + \frac{3}{2}\right), \quad \sigma_l^2 = \frac{1}{N} \left(L + \frac{1}{2}\right), \quad \sigma_d^2 = \frac{1}{N} \left(L + \frac{1}{4}\right), \quad (94)$$

whereas under HRR and also under the random binding, assuming  $N \gg 1$ ,

$$\sigma_s^2 = \frac{1}{N} (L + 3), \quad \sigma_l^2 = \frac{1}{N} (L + 2), \quad \sigma_d^2 = \frac{1}{N} (L + 1). \quad (95)$$

## A.5 Estimation of $\mathbf{a}$ -dependent terms in the variance

Here, we estimate the expectation of  $a_i^\mu a_{i'}^\mu a_l^\rho a_{l'}^\rho / (\sum_{k=1}^N a_k^1 a_k^1)^2$  over random Gaussian vectors  $\mathbf{a}$  under  $N \gg 1$ . First, for  $\mu \geq 2$ , we get,

$$\begin{aligned} &\left\langle \frac{1}{\left(\sum_{k=1}^N a_k^1 a_k^1\right)^2} a_i^\mu a_{i'}^\mu a_l^\rho a_{l'}^\rho \right\rangle \\ &= (\delta_{ii'} \delta_{ll'} + \delta_{\mu\rho} [\delta_{il} \delta_{i'l'} + \delta_{i'l} \delta_{i'l'}]) \left\langle \frac{1}{\left(\sum_k a_k^1 a_k^1\right)^2} \right\rangle + \delta_{1\rho} \delta_{ii'} \delta_{ll'} \left( \left\langle \frac{a_l^1 a_l^1}{\left(\sum_k a_k^1 a_k^1\right)^2} \right\rangle - \left\langle \frac{1}{\left(\sum_k a_k^1 a_k^1\right)^2} \right\rangle \right) \\ &= \frac{1}{(N-2)(N-4)} (\delta_{ii'} \delta_{ll'} + \delta_{\mu\rho} [\delta_{il} \delta_{i'l'} + \delta_{i'l} \delta_{i'l'}]) - \frac{4\delta_{1\rho} \delta_{ii'} \delta_{ll'}}{N(N-2)(N-4)}. \end{aligned} \quad (96)$$

In the last line, we used

$$\begin{aligned} \left\langle \frac{1}{(\sum_k a_k^1 a_k^1)^2} \right\rangle_a &= \left\langle \frac{1}{x^2} \right\rangle_{x \sim \chi_N^2} = \frac{1}{(N-2)(N-4)}, \\ \left\langle \frac{a_l^1 a_l^1}{(\sum_k a_k^1 a_k^1)^2} \right\rangle_a &= \left\langle \frac{x}{(x+y)^2} \right\rangle_{x \sim \chi_1^2, y \sim \chi_{N-1}^2} = \frac{1}{N(N-2)}, \end{aligned} \quad (97)$$

where  $\chi_k^2$  is the chi-squared distribution with degree  $k$ . Similarly, under  $\mu = 1$ ,

$$\begin{aligned} \left\langle \frac{1}{(\sum_k a_k^1 a_k^1)^2} a_i^\mu a_{i'}^\mu a_l^\rho a_{l'}^\rho \right\rangle &\approx (1 - \delta_{1\rho}) \delta_{ii'} \delta_{ll'} \left\langle \frac{a_l^1 a_l^1}{(\sum_k a_k^1 a_k^1)^2} \right\rangle + \delta_{1\rho} (\delta_{ii'} \delta_{ll'} + \delta_{il} \delta_{i'l'} + \delta_{il'} \delta_{i'l}) \left\langle \frac{a_i^1 a_i^1 a_l^1 a_l^1}{(\sum_k a_k^1 a_k^1)^2} \right\rangle \\ &= \frac{(1 - \delta_{1\rho}) \delta_{ii'} \delta_{ll'}}{N(N-2)} + \frac{\delta_{1\rho} (\delta_{ii'} \delta_{ll'} + \delta_{il} \delta_{i'l'} + \delta_{il'} \delta_{i'l})}{N(N+2)}. \end{aligned} \quad (98)$$

In the last line, we used

$$\left\langle \frac{a_i^1 a_i^1 a_l^1 a_l^1}{(\sum_k a_k^1 a_k^1)^2} \right\rangle = \left\langle \frac{xy}{(x+y+z)^2} \right\rangle_{x, y \sim \chi_1^2, z \sim \chi_{N-2}^2} = \frac{1}{N(N+2)}. \quad (99)$$

Therefore, up to the leading order terms,

$$\left\langle \frac{1}{(\sum_k a_k^1 a_k^1)^2} a_i^\mu a_{i'}^\mu a_l^\rho a_{l'}^\rho \right\rangle = \begin{cases} \frac{\delta_{ii'} \delta_{ll'} + \delta_{\mu\rho} (\delta_{il} \delta_{i'l'} + \delta_{il'} \delta_{i'l})}{(N-2)(N-4)} & \mu \geq 2 \\ \frac{\delta_{ii'} \delta_{ll'}}{N(N-2)} + \frac{\delta_{1\rho} (\delta_{il} \delta_{i'l'} + \delta_{il'} \delta_{i'l})}{N(N+2)} & \mu = 1. \end{cases} \quad (100)$$

## A.6 Performance of the random binding

We construct a random binding tensor by setting  $P = Q = R$ , and choosing their elements from i.i.d Gaussian with the mean zero and the variance  $\frac{1}{NN_c}$ . Under this normalization,  $P$  satisfies Eq. 68 under  $N, N_c \gg 1$ . From Eq. 49, the average error over randomly chosen  $P$  is given as

$$\ell_a = \frac{LN}{N_c} \left( 1 + \frac{N_c + 1}{N^2} \right) + \left( \frac{1}{N} + \frac{3}{N_c} + \frac{1}{NN_c} \right). \quad (101)$$

If  $N_c \ll N^2$ , the leading order term is  $\ell_a \approx \frac{LN}{N_c}$ , which is the same with the lower bound. On the other hand, at  $N_c = N^2$  limit, the leading order term becomes  $\ell_a \approx \frac{2LN}{N_c}$ , which is twice larger than that of the tensor product representation (Eq. 145).

## B $K$ -compositional binding and its extensions

### B.1 Sufficiency of the Hurwitz matrix equations for the fixed-point condition

Here we show that Hurwitz matrix equations  $P_j P_i^T + P_i P_j^T = 2\lambda \delta_{ij} I_N$  with  $\lambda = \frac{1}{LN+2}$  are sufficient for the fixed-point conditions with respect to both  $\ell_a$  (Eq. 52) and  $\ell_b$  (Eq. 55) under  $P = Q = R$  constraint. Recall that,  $L$  is the number of bound pairs in the composition. Although we mainly focused on  $L = 1$  in the main text, below we prove the results for arbitrary  $L$ . Firstly, taking the trace of the Hurwitz matrix equations, we get  $\text{tr} [P_i P_j^T] = \lambda N \delta_{ij}$ . Moreover, because  $P_i$  is a square matrix,  $P_i P_i^T = \lambda I_N$  implies  $P_i^T P_i = \lambda I_N$ . Thus,

$$\begin{aligned} \sum_{j=1}^N (\text{tr} [P_j P_i^T] I_N + L P_i P_j^T + P_j P_i^T) P_j &= \sum_{j=1}^N (\lambda N \delta_{ij} I_N + 2\lambda \delta_{ij} I_N) P_j + (L-1) P_i \sum_{j=1}^N P_j^T P_j \\ &= \lambda (LN+2) P_i = P_i. \end{aligned} \quad (102)$$

Secondly, using  $\sum_j (P_j P_i^T + P_i P_j^T) P_j = 2\lambda P_i$ ,

$$\begin{aligned} \sum_j (LP_i P_j^T P_j + P_j P_i^T P_j + P_j P_j^T P_i) &= (L-1) P_i \sum_{j=1}^N P_j^T P_j + \sum_{j=1}^N [P_i P_j^T + P_j P_i^T] P_j + \sum_{j=1}^N P_j P_j^T P_i \\ &= \lambda(LN+2) P_i = P_i. \end{aligned} \quad (103)$$

Hence, a family of matrices  $\{P_i\}_{i=1}^N$  satisfying Eq. 22 also satisfies Eqs. 52 and 55. In particular, under  $L=1$ , it satisfies Eqs. 20 and 21.

## B.2 Octonion binding

Using the Cayley-Dickson construction, a matrix representation of an element  $a = (a_1, a_2, \dots, a_8)$  of the octonion algebra is given as (Tian, 2000)

$$\phi(a) = \begin{pmatrix} a_1 & -a_2 & -a_3 & -a_4 & -a_5 & -a_6 & -a_7 & -a_8 \\ a_2 & a_1 & a_4 & -a_3 & a_6 & -a_5 & -a_8 & a_7 \\ a_3 & -a_4 & a_1 & a_2 & a_7 & a_8 & -a_5 & -a_6 \\ a_4 & a_3 & -a_2 & a_1 & a_8 & -a_7 & a_6 & -a_5 \\ a_5 & -a_6 & -a_7 & -a_8 & a_1 & a_2 & a_3 & a_4 \\ a_6 & a_5 & -a_8 & a_7 & -a_2 & a_1 & -a_4 & a_3 \\ a_7 & a_8 & a_5 & -a_6 & -a_3 & a_4 & a_1 & -a_2 \\ a_8 & -a_7 & a_6 & a_5 & -a_4 & -a_3 & a_2 & a_1 \end{pmatrix}. \quad (104)$$

Because octonions are not associative under multiplication (i.e. there are octonions  $a, b, c$ , such that  $a \cdot (b \cdot c) \neq (a \cdot b) \cdot c$ ), a matrix representation of an octonion is not faithful, unlike matrix representations of the quaternions and the complex numbers. However, from  $\phi(a)$ , we can still construct a family of matrices  $P = [P_1, \dots, P_8]$  that satisfies the Hurwitz matrix equations which we can use as the basis of binding matrices. Under this binding, up to a constant factor, the composition  $c$  of two elements is calculated as

$$\begin{aligned} c_1 &= a_1 b_1 + a_2 b_2 + a_3 b_3 + a_4 b_4 + a_5 b_5 + a_6 b_6 + a_7 b_7 + a_8 b_8, \\ c_2 &= a_1 b_2 - a_2 b_1 + a_3 b_4 - a_4 b_3 + a_5 b_6 - a_6 b_5 - a_7 b_8 + a_8 b_7, \\ c_3 &= a_1 b_3 - a_2 b_4 - a_3 b_1 + a_4 b_2 + a_5 b_7 + a_6 b_8 - a_7 b_5 - a_8 b_6, \\ c_4 &= a_1 b_4 + a_2 b_3 - a_3 b_2 - a_4 b_1 + a_5 b_8 - a_6 b_7 + a_7 b_6 - a_8 b_5, \\ c_5 &= a_1 b_5 - a_2 b_6 - a_3 b_7 - a_4 b_8 - a_5 b_1 + a_6 b_2 + a_7 b_3 + a_8 b_4, \\ c_6 &= a_1 b_6 + a_2 b_5 - a_3 b_8 + a_4 b_7 - a_5 b_2 - a_6 b_1 - a_7 b_4 + a_8 b_3, \\ c_7 &= a_1 b_7 + a_2 b_8 + a_3 b_5 - a_4 b_6 - a_5 b_3 + a_6 b_4 - a_7 b_1 - a_8 b_2, \\ c_8 &= a_1 b_8 - a_2 b_7 + a_3 b_6 + a_4 b_5 - a_5 b_4 - a_6 b_3 + a_7 b_2 - a_8 b_1. \end{aligned}$$

Note that, because matrix representation of octonions is not unique, there are various different ways to construct binding matrices that have octonion structure.

## B.3 Properties of the sparse $K$ -compositional bindings

In Eq. 30, we generated sparse  $K$ -compositional binding operators by a block-wise binding. However, there are many equivalent binding operators due to invariance. In particular, we can generate a family of binding operators using an  $N \times N$  orthogonal matrix  $W$  ( $WW^T = W^T W = I_N$ ). Let us denoting  $A = \{A_1, \dots, A_K\}$  as a family of  $K \times K$  matrices that satisfies the Hurwitz matrix equations

$$A_i A_j^T + A_j A_i^T = 2\lambda \delta_{ij} I_K \quad (105)$$



for  $i, j = 1, \dots, K$ , with the normalization factor:

$$\lambda = \frac{1}{LK + 2}. \quad (106)$$

Setting  $N = qK$  with a natural number  $q$ , we construct a binding operator  $P_n$  ( $n = 1, \dots, N$ ) by

$$P_n = \left( \sum_{k=1}^K W_{n,k} A_k \right) \oplus \left( \sum_{k=1}^K W_{n,K+k} A_k \right) \oplus \dots \oplus \left( \sum_{k=1}^K W_{n,(q-1)K+k} A_k \right). \quad (107)$$

In other words, we set the  $r$ -th block diagonal component of  $P_n$  to  $\sum_{k=1}^K W_{n,(r-1)K+k} A_k$ . If we choose  $W = I_N$ , we recover Eq. 30. Below we show that under this binding, for arbitrary positive integer  $L$ , the decoding error becomes  $\ell_a = \ell_b = \frac{(L-1)K+2}{LK+2}$  and  $\{P_n\}_{n=1}^N$  satisfies the fixed-point conditions for both  $\ell_a$  and  $\ell_b$ . In particular, we recover  $\ell_a = \ell_b = \frac{2}{K+2}$  under  $L = 1$ .

**Decoding error of  $\mathbf{a}$**  Here we show that, under this binding, the error  $\ell_a$  (Eq. 50) satisfies  $\ell_a = \frac{(L-1)K+2}{LK+2}$ . Firstly, using  $\text{tr}[A_k A_n^T] = \lambda K \delta_{kn}$ ,  $\text{tr}[P_i P_l^T]$  becomes

$$\begin{aligned} \text{tr}[P_i P_l^T] &= \sum_{r=0}^{q-1} \text{tr} \left[ \left( \sum_{k=1}^K W_{i,rK+k} A_k \right) \left( \sum_{n=1}^K W_{l,rK+n} A_n^T \right) \right] \\ &= \lambda K \sum_{r=0}^{q-1} \sum_{k=1}^K W_{i,rK+k} W_{l,rK+n} \\ &= \lambda K [W W^T]_{il} = \lambda K \delta_{il}. \end{aligned} \quad (108)$$

In the last line, we used the fact that  $W$  is an orthogonal matrix. Similarly, using  $A_i A_j^T + A_j A_i^T = 2\lambda \delta_{ij} I_K$ ,

$$\begin{aligned} &\sum_{i=1}^N \sum_{l=1}^N \text{tr}[P_l P_i^T (P_l P_i^T + P_i P_l^T)] \\ &= \sum_{i=1}^N \sum_{l=1}^N \sum_{r=0}^{q-1} \left[ \sum_{k=1}^K \sum_{k'=1}^K W_{l,rK+k} W_{i,rK+k'} A_k A_{k'}^T \sum_{n=1}^K \sum_{n'=1}^K W_{l,rK+n} W_{i,rK+n'} (A_n A_{n'}^T + A_{n'} A_n^T) \right] \\ &= 2\lambda^2 K \sum_{r=0}^{q-1} \sum_{k=1}^K \sum_{n=1}^K \left( [W^T W]_{rK+k, rK+n} \right)^2 \\ &= 2\lambda^2 NK. \end{aligned} \quad (109)$$

Finally,

$$\begin{aligned} \sum_{i=1}^N \sum_{l=1}^N \text{tr}[P_l P_i^T P_i P_l^T] &= \sum_{r=0}^{q-1} \sum_{k=1}^K \sum_{m=1}^K \sum_{k'=1}^K \sum_{m'=1}^K [W^T W]_{rK+k, rK+k'} [W^T W]_{rK+m, rK+m'} \text{tr}[A_k A_m^T A_{m'} A_{k'}^T] \\ &= \sum_{r=0}^{q-1} \sum_{k=1}^K \sum_{m=1}^K \text{tr}[A_k A_m^T A_m A_k^T] \\ &= N\lambda^2 K^2. \end{aligned} \quad (110)$$

Therefore, from Eq. 50, the loss  $\ell_a$  becomes

$$\ell_a = 1 - 2\lambda K + (\lambda K)^2 + 2\lambda^2 K + (L-1)\lambda^2 K^2 = \frac{(L-1)K+2}{LK+2}. \quad (111)$$

Moreover, the binding operator defined by Eq. 107 satisfies the fixed-point condition, Eq. 52. First, from Eq. 108,

$$\sum_{l=1}^N \text{tr} [P_l P_l^T] I_N P_l = \lambda K P_i. \quad (112)$$

$(r+1)$ -th diagonal block component of  $\sum_l [P_l P_l^T + P_i P_l^T] P_l$  is written as

$$\begin{aligned} \left[ \sum_{l=1}^N (P_l P_l^T + P_i P_l^T) P_l \right]_{(r+1)\text{-th block}} &= \sum_{l=1}^N \left( \sum_{k=1}^K \sum_{m=1}^K W_{l,rK+k} W_{i,rK+m} [A_k A_m^T + A_m A_k^T] \right) \left( \sum_{n=1}^N W_{l,rK+n} A_n \right) \\ &= 2\lambda \sum_{k=1}^K \sum_{n=1}^K W_{i,rK+k} \left( \sum_{l=1}^N W_{l,rK+k} W_{l,rK+n} \right) A_n \\ &= 2\lambda [P_i]_{(r+1)\text{-th block}}. \end{aligned} \quad (113)$$

In addition, we have

$$\begin{aligned} \sum_{l=1}^N [P_l P_l^T]_{(r+1)\text{-th block}} &= \sum_{i=1}^N \left( \sum_{k=1}^K W_{l,rK+k} A_k \right) \left( \sum_{n=1}^K W_{l,rK+n} A_n^T \right) \\ &= \sum_{k=1}^K \sum_{n=1}^K [W^T W]_{rK+k, rK+n} A_k A_n^T = K \lambda I_K, \end{aligned} \quad (114)$$

By combining the equations above, we get

$$\sum_{l=1}^N (\text{tr} [P_l P_l^T] I_N + L \cdot P_i P_l^T + P_l P_i^T) P_l = (\lambda K + 2\lambda + [L-1] \lambda K) P_i = P_i. \quad (115)$$

Thus, Eq. 107 indeed satisfies the fixed-point condition, Eq. 52.

**Decoding error of  $\mathbf{b}$**  Let us next consider the decoding error of  $\mathbf{b}$ ,  $\ell_b$ . Under  $P = R$ , the error  $\ell_b$  is written as

$$\ell_b = 1 - \frac{2}{N} \sum_i \text{tr} [P_i P_i^T] + \frac{1}{N} \sum_i \sum_l (\text{tr} [P_i P_i^T P_l P_l^T] + \text{tr} [P_l P_i^T (L \cdot P_i P_l^T + P_l P_i^T)]). \quad (116)$$

From Eq. 114, we get

$$\sum_{i=1}^N \sum_{l=1}^N \text{tr} [P_i P_i^T P_l P_l^T] = \text{tr} [(K\lambda)^2 I_N] = NK^2 \lambda^2. \quad (117)$$

Because the rest of terms are the same with  $\ell_a$ , the error  $\ell_b$  also follows

$$\ell_b = 1 - 2K\lambda_K + K^2 \lambda_K^2 + 2K\lambda_K^2 + (L-1) \lambda^2 K^2 = \frac{(L-1)K+2}{LK+2}. \quad (118)$$

Moreover,  $\{P_i\}_{i=1}^N$  constructed by Eq. 107 satisfies the fixed-point condition Eq. 55. From Eqs. 113 and 114, it follows that

$$\begin{aligned} \sum_{l=1}^N (L \cdot P_i P_l^T P_l + P_l P_i^T P_l + P_l P_l^T P_i) &= (L-1) P_i \sum_l P_l^T P_l + \sum_l (P_i P_l^T + P_l P_i^T) P_l + \sum_l P_l P_l^T P_i \\ &= (L-1) \lambda K P_i + 2\lambda P_i + \lambda L P_i = P_i. \end{aligned} \quad (119)$$

## B.4 Extended octonion binding

The sparse octonion binding can be naturally extended to  $N_c > N$  when  $N_c$  satisfies  $N_c = dN$  for a positive integer  $d$ . As before, we set  $N$  to be  $N = qK$  for a positive integer  $q$ .

Let us focus on the case when  $N_c < N^2/K$  for simplicity. Using a solution for Eq. 105,  $\{A_i\}_{i=1}^K$ , we introduce a family of  $N \times N$  matrix  $\{B^{\mu\nu}\}$  as

$$B^{\mu\nu} \equiv \underbrace{O_K \oplus \dots \oplus O_K}_{\nu} \oplus A_\mu \oplus O_K \oplus \dots \oplus O_K \quad (120)$$

for  $\mu = 1, \dots, K$  and  $\nu = 0, \dots, q-1$ . We then construct a family of  $N \times N_c$  matrices  $\{P_i\}_{i=1}^N$  from  $B$  as

$$P_i = \left[ B^{\lceil i/q \rceil, i \% q}, B^{\lceil i/q \rceil, (i+1) \% q}, \dots, B^{\lceil i/q \rceil, (i+d-1) \% q} \right]. \quad (121)$$

For instance, if  $q = 3$  and  $d = 2$ , then

$$\begin{aligned} P_1 &= \begin{pmatrix} A_1 & O & O & O & O & O \\ O & O & O & O & A_1 & O \\ O & O & O & O & O & O \end{pmatrix}, & P_2 &= \begin{pmatrix} O & O & O & O & O & O \\ O & A_1 & O & O & O & O \\ O & O & O & O & O & A_1 \end{pmatrix}, \\ P_3 &= \begin{pmatrix} O & O & O & A_1 & O & O \\ O & O & O & O & O & O \\ O & O & A_1 & O & O & O \end{pmatrix}, & P_4 &= \begin{pmatrix} A_2 & O & O & O & O & O \\ O & O & O & O & A_2 & O \\ O & O & O & O & O & O \end{pmatrix}, \dots \end{aligned} \quad (122)$$

Let us estimate the error under this binding method. From the definition,  $P_i P_l^T$  is written as

$$P_i P_l^T = \sum_{r=0}^{d-1} [(i+r) \% q = (l+r) \% q]_+ \underbrace{O_K \oplus \dots \oplus O_K}_{(i+r) \% q} \oplus A_{\lceil i/q \rceil} A_{\lceil l/q \rceil}^T \oplus O_K \oplus \dots \oplus O_K, \quad (123)$$

where  $[x]_+$  is an indicator function that returns 1 if  $x$  is true, and returns 0 if false. Thus,  $\text{tr} [P_i P_i^T] = d\lambda_K K$ . This means that, in order to satisfy Eq. 68, the scaling factor  $\lambda_K$  of  $A_k$  in Eq. 105 needs to be  $\lambda_K = 1/(dK)$ . The dominant term of the error becomes

$$\begin{aligned} \frac{L}{N} \sum_{i=1}^N \sum_{l=1}^N \text{tr} [P_l P_i^T P_i P_l^T] &= \frac{L}{N} \sum_{i=1}^N \sum_{l=1}^N \sum_{r=0}^{d-1} [(i+r) \% q = (l+r) \% q]_+ \text{tr} \left[ A_{\lceil l/q \rceil} A_{\lceil i/q \rceil}^T A_{\lceil i/q \rceil} A_{\lceil l/q \rceil}^T \right] \\ &= \frac{L}{N} \sum_{r=0}^{d-1} \sum_{m=1}^q \sum_{k=1}^K \sum_{m'=1}^q \sum_{k'=1}^K [([k-1]q + m) \% q = ([k'-1]q + m') \% q]_+ \text{tr} [A_{k'} A_k^T A_k A_{k'}^T] \\ &= \frac{L}{N} \sum_{r=0}^{d-1} \sum_{m=1}^q \sum_{m'=1}^q [m \% q = m' \% q]_+ (\lambda_K K)^2 K \\ &= \frac{L}{N} \frac{dN}{K} \lambda_K^2 K^3 = \frac{LN}{N_c} \end{aligned} \quad (124)$$

Therefore, the dominant term is the same with the lower bound obtained in Appendix A.3. Calculating the rest of terms in a similar manner, we get

$$\ell_a = \frac{N}{N_c} \left( L - 1 + \frac{2}{K} \right). \quad (125)$$

## B.5 Construction of higher-order sparse $K$ -compositional bindings

In the simulations depicted in Figs 4,5,7-9, we constructed sparse  $K$ -compositional bindings by using a python library for the Cayley-Dickson construction, developed by Dr. Travis Hoppe (<https://github.com/thoppe/Cayley-Dickson>). Source codes for the simulations are available at [https://github.com/nhiratani/quadratic\\_binding](https://github.com/nhiratani/quadratic_binding).

## C Tensor-HRR bindings

Below, we review two commonly used binding mechanisms: holographic reduced representation (HRR) (Plate, 1995, 1997; Nickel et al., 2016) and tensor product representation (Smolensky, 1990; Smolensky et al., 2014). Subsequently, we introduce a binding that morphs from HRR to the tensor product representation as you change the vector length of the representation.

### C.1 Holographic reduced representation (HRR)

Under HRR, the length of the composition vector  $\mathbf{c}$  is the same with that of  $\mathbf{a}$  and  $\mathbf{b}$  ( $N_c = N$ ), and the  $k$ -th element of binding  $\psi$  is constructed by

$$\psi_k(\mathbf{a}_\mu, \mathbf{b}_\mu) = \sum_{i=1}^N a_i^\mu b_{[k-i]_N}^\mu \text{ for } k = 1, \dots, N \quad (126)$$

where  $[k-i]_N \equiv k-i \pmod{N}$ , and  $a_i^\mu$  is the  $i$ -th element of vector  $\mathbf{a}_\mu$ . Given  $\mathbf{c} = \sum_{\mu=1}^L \psi(\mathbf{a}_\mu, \mathbf{b}_\mu)$ , we can unbind  $\mathbf{a}_1$  from  $\mathbf{c}$  using a query  $\mathbf{b}_1$  as

$$\hat{a}_i^1 = \frac{1}{\|\mathbf{b}_1\|^2} \sum_{j=1}^N c_{[j+i]_N} b_j^1. \quad (127)$$

Because  $\mathbf{c}$  is rewritten as

$$c_k = \sum_{\mu=1}^L \sum_{i=1}^N a_i^\mu b_{[k-i]_N}^\mu = \sum_{\mu=1}^L \sum_{i=1}^N \sum_{j=1}^N a_i^\mu b_j^\mu \delta_{[i+j]_N, k}, \quad (128)$$

this is a quadratic binding with

$$P_{ijk} = \delta_{[i+j]_N, k}. \quad (129)$$

Similarly, if the amplitude of  $\mathbf{a}_\mu$  and  $\mathbf{b}_\mu$  are normalized as  $\|\mathbf{a}_\mu\|^2 = \|\mathbf{b}_\mu\|^2 = N$ , unbinding of  $\mathbf{a}$  and  $\mathbf{b}$  are given as

$$Q_{ijk} = R_{ijk} = \frac{1}{N} \delta_{[i+j]_N, k}. \quad (130)$$

Alternatively, by moving the half of the normalization factor to the binding operator, we can rewrite  $P, Q, R$  as

$$P_{ijk} = Q_{ijk} = R_{ijk} = \frac{1}{\sqrt{N}} \delta_{[i+j]_N, k}. \quad (131)$$

Under both normalizations, the amplitude of the recovered signal becomes the same with the original signal amplitude (see Eq. 67). However, this normalization does not necessarily minimize the mean-squared error  $\ell_a$  and  $\ell_b$ . To see this, let us define  $P_{ijk} = Q_{ijk} = R_{ijk} = \sqrt{\lambda} \delta_{[i+j]_N, k}$  where  $\lambda$  is a scaling factor. Then, from Eq. 10, assuming that  $N$  is an even number, the loss  $\ell_a$  becomes

$$\ell_a = 1 - 2N\lambda + ((L+1)N+2)N\lambda^2. \quad (132)$$

Thus, the loss is minimized at  $\lambda = \frac{1}{(L+1)N+2}$ , under which the loss follows  $\ell_a = \frac{LN+2}{(L+1)N+2}$ . In particular, when only one pair is bound to the composition ( $L=1$ ), we get  $\ell_a = \frac{N+2}{2(N+1)}$  (blue line in Fig. 4A), and taking the large  $N$  limit, we obtain  $\ell_a = \frac{1}{2}$  (gray dashed line in Fig. 2A and B). If we instead set  $\lambda = \frac{1}{N}$  to make the decoding unbiased, the loss follows  $\ell_a = 1 + \frac{2}{N}$  under  $L=1$  (blue line in Fig. 4C). The loss  $\ell_b$  becomes the same due to the symmetry between  $\mathbf{a}$  and  $\mathbf{b}$  under HRR (Eq. 131 is invariant against  $i \leftrightarrow j$ ).

It should be noted that HRR does not satisfy the fixed-point conditions (Eqs. 52 and 55) under a finite  $N$  regardless of the choice of the scaling factor. This is because the right-hand side of Eq. 20 becomes

$$\sum_{l=1}^N (\text{tr} [P_l P_l^T] I_N + L \cdot P_l P_l^T + P_l P_l^T) P_l = \lambda(L+1)NP_i + \lambda P_i^{res}, \quad (133)$$

where  $[P_i^{res}]_{jk} \equiv \sqrt{\lambda} \sum_l \delta_{[2l]_N, [i-j+k]_N}$ . Nonetheless, the fact that  $P = Q$  is satisfied under HRR is consistent with the condition on the optimal  $Q$  at  $L \gg 1$  limit (Eq. 72). Under HRR,

$$\left[ \sum_{l=1}^N P_l P_l^T \right]_{jm} = \sum_{l=1}^N \sum_{k=1}^N P_{ljk} P_{lmk} = \frac{1}{N} \sum_{l=1}^N \delta_{[l+j]_N, [l+m]_N} = \delta_{jm}. \quad (134)$$

Thus, for a given  $P$ , to minimize the Lagrangian,  $Q$  needs to satisfy  $Q_i = \lambda_i P_i$  for  $i = 1, \dots, N$ . This result supports the optimality of unbinding by circular correlation given a binding by circular convolution at  $L \gg 1$ . From the symmetry between  $\mathbf{a}$  and  $\mathbf{b}$  ( $P_{ijk} = P_{jik}$ ), we expect  $R_i = \lambda_i P_i$  to be the optimal too at  $L \gg 1$ .

## C.2 Tensor product representation

In the tensor product representation,  $S = \{(\mathbf{a}_\mu, \mathbf{b}_\mu)\}_{\mu=1}^L$  is represented by a  $N \times N$  matrix  $\mathbf{C}$ :

$$\mathbf{C} = \sum_{\mu=1}^L \mathbf{a}_\mu \mathbf{b}_\mu^T \quad (135)$$

Alternatively, we can consider  $\mathbf{C}$  as a length  $N_c = N^2$  vector  $\mathbf{c} = \text{Vec}[\mathbf{C}]$ . Given  $\mathbf{C}$  and a query  $\mathbf{b}_1$ , unbinding of  $\mathbf{a}_1$  is done by

$$\hat{\mathbf{a}}_1 = \frac{1}{\|\mathbf{b}_1\|^2} \mathbf{C} \mathbf{b}_1 \quad (136)$$

This unbinding is lossless if  $L = 1$  because  $\frac{1}{\|\mathbf{b}_1\|^2} \mathbf{a}_1 \mathbf{b}_1^T \mathbf{b}_1 = \mathbf{a}_1$ . The tensor product representation is also an example of quadratic binding family in which, assuming  $\|\mathbf{a}_\mu\|^2 = \|\mathbf{b}_\mu\|^2 = N$ , the tensors  $P, Q, R$  are set to

$$P_{ijk} = Q_{ijk} = R_{ijk} = \frac{1}{\sqrt{N}} \delta_{k, (iN+j)}. \quad (137)$$

Notably,  $P = Q = R$  is satisfied in the tensor product representation too.

## C.3 Tensor-HRR morphing

For  $N_c = dN$  with  $d = 1, 2, \dots, N$ , we define tensor-HRR binding as

$$P_{ijk} = Q_{ijk} = R_{ijk} = \frac{1}{\sqrt{N}} \delta_{[id+j]_{dN}, k} \quad (138)$$

At  $N_c = N$  ( $d = 1$ ), this is the same with HRR (Eq. 131), whereas at  $N_c = N^2$ ,  $\delta_{[iN+j]_{N^2}, k} = \delta_{(iN+j), k}$ , thus it becomes the tensor-product binding (Eq. 137). Noticing that  $M$  (Eq. 45) is written as

$$M_{mj}^{li} = \frac{1}{N} \delta_{[id+j]_{dN}, [ld+m]_{dN}}, \quad (139)$$

unbinding of  $\mathbf{a}_1$  indeed yields

$$\begin{aligned} \langle \hat{\mathbf{a}}_i^1 \rangle_{p(b)} &= \left\langle \sum_j \sum_k P_{ijk} b_j^1 \sum_\mu \sum_l \sum_m P_{lmk} a_l^\mu b_m^\mu \right\rangle_{p(b)} \\ &= \left\langle \sum_j \sum_l M_{jj}^{li} (b_j^1)^2 a_l^1 \right\rangle_{p(b)} \\ &= \frac{1}{N} \sum_j \sum_l \delta_{[id+j]_{dN}, [ld+j]_{dN}} a_l^1 \\ &= a_i^1. \end{aligned} \quad (140)$$

In the last line, we used

$$id + j \equiv ld + j \pmod{dN} \Leftrightarrow (i-l)d \equiv 0 \pmod{dN} \Leftrightarrow i = l, \quad (141)$$

for  $i, l = 1, \dots, N$ . The decoding error (Eq. 49) under this binding is estimated as below. First, from Eq. 139

$$1 - \frac{2}{N} \sum_i \sum_j M_{jj}^{ii} + \frac{1}{N} \sum_i \sum_l \left( \sum_j M_{jj}^{li} \right)^2 = 1 - 2 + 1 = 0. \quad (142)$$

On the other hand, under  $N \gg 1$ , the noise term is given as

$$\begin{aligned} \frac{1}{N} \sum_i \sum_l \sum_j \sum_m M_{mj}^{li} (LM_{mj}^{li} + M_{mj}^{il}) &= \frac{1}{N^3} \sum_i \sum_l \sum_j \sum_m (L\delta_{[id+j]_{dN}, [ld+m]_{dN}} + \delta_{[id+j]_{dN}, [ld+m]_{dN}} \delta_{[ld+j]_{dN}, [id+m]_{dN}}) \\ &\approx \frac{L}{d} + \frac{1}{N}. \end{aligned} \quad (143)$$

The last line follows under a large  $N$ , because for randomly sampled integers  $1 \leq i, l, j, m \leq N$ ,

$$\Pr [\delta_{[id+j]_{dN}, [ld+m]_{dN}} = 1] = \frac{1}{dN}. \quad (144)$$

Combining the terms above, we get

$$\ell_a \approx \frac{LN}{N_c} + \frac{1}{N}. \quad (145)$$

## Data availability

Source code is available at [https://github.com/nhiratani/quadratic\\_binding](https://github.com/nhiratani/quadratic_binding).

## Acknowledgements

This work has been supported by the Swartz Foundation.

## References

- Aerts, D., Czachor, M., and De Moor, B. (2009). Geometric analogue of holographic reduced representation. *Journal of Mathematical Psychology*, 53(5):389–398.
- Antol, S., Agrawal, A., Lu, J., Mitchell, M., Batra, D., Zitnick, C. L., and Parikh, D. (2015). Vqa: Visual question answering. In *Proceedings of the IEEE international conference on computer vision*, pages 2425–2433.
- Baez, J. (2002). The octonions. *Bulletin of the american mathematical society*, 39(2):145–205.
- Cowan, N. (2001). The magical number 4 in short-term memory: A reconsideration of mental storage capacity. *Behavioral and brain sciences*, 24(1):87–114.
- Eliasmith, C., Stewart, T. C., Choo, X., Bekolay, T., DeWolf, T., Tang, Y., and Rasmussen, D. (2012). A large-scale model of the functioning brain. *science*, 338(6111):1202–1205.
- Feldman, J. (2013). The neural binding problem (s). *Cognitive neurodynamics*, 7(1):1–11.
- Frady, E. P., Kleyko, D., and Sommer, F. T. (2020). Variable binding for sparse distributed representations: Theory and applications. *arXiv preprint arXiv:2009.06734*.
- Gallant, S. I. and Okaywe, T. W. (2013). Representing objects, relations, and sequences. *Neural computation*, 25(8):2038–2078.
- Gayler, R. W. (2004). Vector symbolic architectures answer jackendoff’s challenges for cognitive neuroscience. *arXiv preprint cs/0412059*.

- Gosmann, J. and Eliasmith, C. (2019). Vector-derived transformation binding: an improved binding operation for deep symbol-like processing in neural networks. *Neural computation*, 31(5):849–869.
- Greff, K., van Steenkiste, S., and Schmidhuber, J. (2020). On the binding problem in artificial neural networks. *arXiv preprint arXiv:2012.05208*.
- Hirokawa, J., Vaughan, A., Masset, P., Ott, T., and Kepecs, A. (2019). Frontal cortex neuron types categorically encode single decision variables. *Nature*, 576(7787):446–451.
- Johnson, J., Hariharan, B., Van Der Maaten, L., Fei-Fei, L., Lawrence Zitnick, C., and Girshick, R. (2017). Clevr: A diagnostic dataset for compositional language and elementary visual reasoning. In *Proceedings of the IEEE conference on computer vision and pattern recognition*, pages 2901–2910.
- Kanerva, P. (2009). Hyperdimensional computing: An introduction to computing in distributed representation with high-dimensional random vectors. *Cognitive computation*, 1(2):139–159.
- Kanerva, P. et al. (1997). Fully distributed representation. *PAT*, 1(5):10000.
- Miller, G. A. (1956). The magical number seven, plus or minus two: Some limits on our capacity for processing information. *Psychological review*, 63(2):81.
- Murdock, B. B. (1982). A theory for the storage and retrieval of item and associative information. *Psychological Review*, 89(6):609.
- Nickel, M., Murphy, K., Tresp, V., and Gabilovich, E. (2015). A review of relational machine learning for knowledge graphs. *Proceedings of the IEEE*, 104(1):11–33.
- Nickel, M., Rosasco, L., and Poggio, T. (2016). Holographic embeddings of knowledge graphs. In *Proceedings of the AAAI Conference on Artificial Intelligence*, volume 30.
- Nieh, E. H., Schottdorf, M., Freeman, N. W., Low, R. J., Lewallen, S., Koay, S. A., Pinto, L., Gauthier, J. L., Brody, C. D., and Tank, D. W. (2021). Geometry of abstract learned knowledge in the hippocampus. *Nature*, 595(7865):80–84.
- Plate, T. (1997). A common framework for distributed representation schemes for compositional structure. *Connectionist systems for knowledge representation and deduction*, pages 15–34.
- Plate, T. A. (1995). Holographic reduced representations. *IEEE Transactions on Neural networks*, 6(3):623–641.
- Rigotti, M., Barak, O., Warden, M. R., Wang, X.-J., Daw, N. D., Miller, E. K., and Fusi, S. (2013). The importance of mixed selectivity in complex cognitive tasks. *Nature*, 497(7451):585–590.
- Santoro, A., Raposo, D., Barrett, D. G., Malinowski, M., Pascanu, R., Battaglia, P., and Lillicrap, T. (2017). A simple neural network module for relational reasoning. *arXiv preprint arXiv:1706.01427*.
- Schlegel, K., Neubert, P., and Protzel, P. (2020). A comparison of vector symbolic architectures. *arXiv preprint arXiv:2001.11797*.
- Shapiro, D. B. (2011). *Compositions of quadratic forms*. de Gruyter.
- Smolensky, P. (1990). Tensor product variable binding and the representation of symbolic structures in connectionist systems. *Artificial intelligence*, 46(1-2):159–216.
- Smolensky, P., Goldrick, M., and Mathis, D. (2014). Optimization and quantization in gradient symbol systems: A framework for integrating the continuous and the discrete in cognition. *Cognitive science*, 38(6):1102–1138.
- Socher, R., Chen, D., Manning, C. D., and Ng, A. (2013). Reasoning with neural tensor networks for knowledge base completion. In *Advances in neural information processing systems*, pages 926–934.

- Steinberg, J. and Sompolinsky, H. (2022). Associative memory of structured knowledge. *bioRxiv*.
- Teney, D., Anderson, P., He, X., and Van Den Hengel, A. (2018). Tips and tricks for visual question answering: Learnings from the 2017 challenge. In *Proceedings of the IEEE conference on computer vision and pattern recognition*, pages 4223–4232.
- Tian, Y. (2000). Matrix representations of octonions and their applications. *arXiv preprint math/0003166*.
- Whittington, J. C., Muller, T. H., Mark, S., Chen, G., Barry, C., Burgess, N., and Behrens, T. E. (2020). The tolman-eichenbaum machine: Unifying space and relational memory through generalization in the hippocampal formation. *Cell*, 183(5):1249–1263.